WP5

Final report on

sites evaluation

and on

shore and deep-sea infrastructure

1. SITE INVESTIGATIONS

The Mediterranean Sea offers optimal conditions, on a worldwide scale, to host an underwater neutrino telescope. Several suitable sites have been identified.

Many physical, geophysical and oceanographycal parameters have been taken into account to study the properties of the sites that are proposed to host the KM3NeT infrastructure, the most relevant of which are:

- Proximity to the coast to ease deployment and reduce the expense of the power and signal cable connections to shore;
- Low risk of seismical events;
- A sufficient depth to reduce background from atmospheric muons, in particular from those that are mis-reconstructed as up-going;
- Good optical properties of the water, i.e. absorption and scattering lengths close to the ones of optically pure sea water for light in the wavelength range of 350 nm to 550 nm;
- Low level of bioluminescence;
- Low rates of biofouling (bacterial film deposition and marine life accretion) on optical surfaces;
- Low rates of sedimentation;
- Stable low sea current velocities.

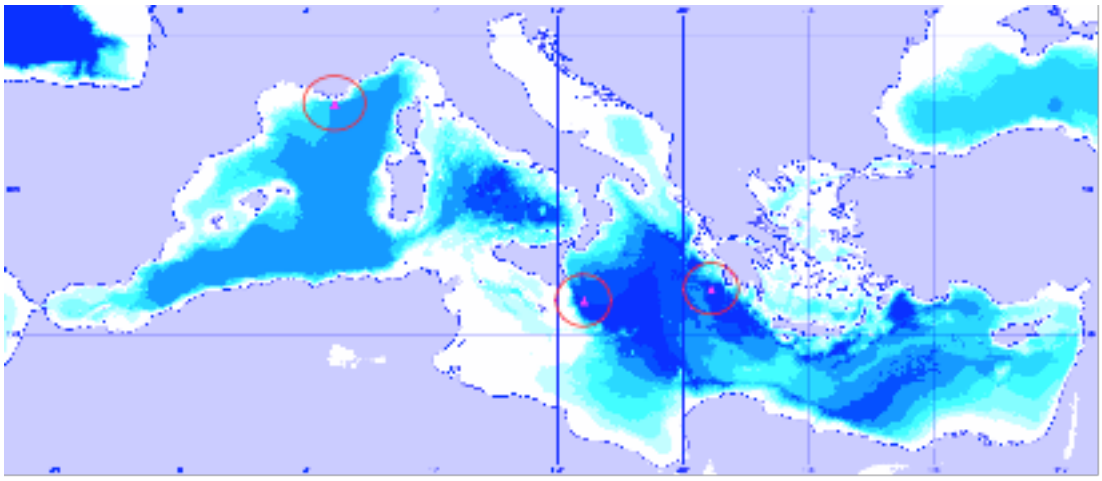

Figure 1 – The three KM3NET sites: from West to East, ANTARES off the south coast of France, NEMO East of Sicily (Italy) and NESTOR west of the Peloponnese (Greece).

The three KM3NET sites: from West to East, ANTARES off the south coast of France, NEMO East of Sicily (Italy) and NESTOR west of the Peloponnese (Greece).

Careful studies of candidate sites have been carried out in order to characterize them. The ANTARES, NEMO and NESTOR Collaborations have carried out dedicated research programmes to characterise the candidate sites, which are currently

pursued within the context of the KM3NeT project. The locations of the three candidate regions, shown in Figure 1, are:

Toulon - Ligurian Sea (ANTARES):

- 42°48' N 06°10' E, depth: 2475 m.

Capo Passero - West Ionian Sea (NEMO):

- 36°16'N 16°06' E, depth: 3500 m.

Pylos - East Ionian Sea (NESTOR):

- 36° 33'N 21°08'E, depth: 5200 m or
- 36° 33'N 21°29'E, depth: 4500 m or
- 36° 38'N 21°35'E, depth: 3750 m.

Deep-sea water optical properties (absorption and diffusion) and environmental properties (water temperature, salinity, biological activity, optical background, water currents and sedimentation) have been studied.

Given the large amount of data collected to date and the ongoing character of these investigations the data presented below are typical examples of the overall sample. The complete set of data will be used to aid in the site selection.

1.1 Water Optical Properties

1.1.1 Light Transmission

The study of the deep-sea water optical properties has been performed through a long-term programme carried out spanning all the seasons. Sea water absorbs and scatters light depending on the water temperature, salinity, as well as the characteristics and concentration of the suspended particulate. These parameters are different at different marine sites and may vary as a function of time.

In order to properly describe the transparency of natural waters, as a function of wavelength, it is necessary to measure the inherent optical properties of the water, such as the absorption length $L_a(\lambda)$, scattering length $L_b(\lambda)$ and attenuation length $1/L_c(\lambda) = 1/L_a(\lambda) + 1/L_b(\lambda)$. Each of these lengths represents the path after which a beam of initial intensity I_0 and wavelength λ is reduced in intensity by a factor of 1/e through absorption, scattering or both according to:

$$I_{a,b,c}(x) = I_0 e^{(-x/L_{a,b,c})}$$

where x is the optical path traversed by the beam. In the literature the coefficients of absorption, $a=1/L_a(\lambda)$ and scattering, $b=1/L_b(\lambda)$, are also used to characterise the light transmission through matter. The sum of scattering and absorption coefficients is called attenuation coefficient c.

Scattering is only taken into account for processes in which the direction of the light is changed without any other alteration. Scattering phenomena in which the photon

wavelength changes (e.g. Raman effect) happen less frequently. Scattering can take place either on molecules (Rayleigh scattering) or on particulate matter (Mie scattering). Other parameters commonly used in the literature are the effective scattering length

$$L_b^{eff} = \frac{L_b(\lambda)}{1-\langle\cos\vartheta\rangle} = \frac{1}{b^{eff}}$$

and the effective attenuation length

$$L_c^{eff} = \frac{1}{c^{eff}} = \frac{1}{a+b^{eff}} \ ,$$

where $\langle\cos\vartheta\rangle$ is the average cosine of the scattering angle. The estimation of the latter parameter is difficult since it needs the knowledge of another inherent optical property, the volume scattering function b(λ,ϑ), that must be measured with appropriate devices.

Using a "non collimated" light beam is also possible to measure the so called "Transmission Length" (L_β) that, in an open geometry experiment characterizes the variation of light intensity as a function of the distance (R) between the source and the detector:

$$I(\lambda,R) = \frac{I_0(\lambda)}{4\pi R^2} e^{-\frac{R}{L_\beta(\lambda)}}$$

under the hypothesis that the light source and the water are fully isotropic.

The "Transmission Length" can be estimated, for specific values of λ) by fitting the behaviour of the *I(λ,R)* in an experiment with data taken with fixed $I_0(\lambda)$ and several values of R.

A direct comparison between measured values of $L_\beta(\lambda)$ and L_c^{eff} would be possible only knowing how to parameterize the diffusion of light in deep sea (i.e. knowing the volume scattering function as a function of λ, or the value of $\langle\cos\vartheta\rangle$) . This knowledge is still lacking for the Mediterranean sea.

Light Transmission Measurements

The Toulon site has been studied for many years with dedicated setups designed to characterise water optical properties. Early measurements [ref. J.A. Aguilar et al. (ANTARES collaboration), Astroparticle Physics, 23(2005)131.] taken between 1997 and 2000 were made for blue (473 nm, with 10 nm of FWHM) and UV (375 nm, with 10 nm of FWHM) light. The results for the absorption, scattering, and effective attenuation lengths are summarised in Table 1-1 and in Table 1-2.

Date	Effective attenuation length (m)	Absorption length (m)	Effective scattering length (m)
July 1998	60.6±0.4± 5	68.6±1.3±5	265±4±28
Mar. 1999	51.9±0.7±1	61.2±0.7±1	228±11±24
June 2000	46.4±1.9±2	49.3±0.3±2	301±3±27

Table 1-1 - Summary of results obtained at the Toulon site using blue light. The first error is statistical and the second one is systematic.

Date	Effective attenuation length (m)	Absorption length (m)	Effective scattering length (m)
July 1999	21.9±0.8±2	23.5±0.1±2	119±2±10
Sept.1999	22.8±0.3±2	25.6±0.2±2	113±3±10
June 2000	26.0±0.5±1	28.9±0.1±1	133±3±12

Table 1-2 - Summary of results at the Toulon site using UV light. The first error is statistical and the second one is systematic.

The ANTARES detector is in operation since few years and the water transmission length is being measured by means of its own instrumentation. Optical beacons (wavelength =470 nm), operated from time to time to perform calibrations, and the Optical Modules placed at several distances allow to measure, in situ, the light transmission as a function of the distance. Fig. 1-1 shows the results of these measurements over nearly 18 months. Monte Carlo simulations indicate that, for reasonable scattering models, the absorption length is typically 5m larger than the transmission length.

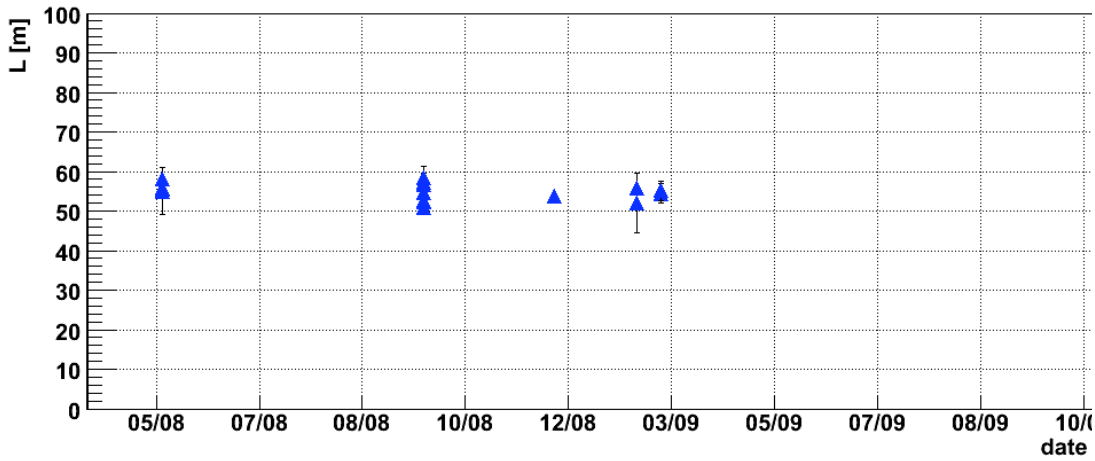

Fig. 1-1 - In situ transmission length measurements in Toulon site. Values are extracted from measurements using the optical beacons (wavelength =470 nm). Monte Carlo simulations indicate that, for reasonable scattering models, the sea water absorption length is typically 5m larger than the measured transmission length.

The Capo Passero site has been investigated [Riccobene, et al., Astroparticle Physics, 27 (2007)1.] using a setup including a commercial instrument (the AC9 by WETLABS) capable of measuring, in a well collimated geometry, the absorption and the attenuation coefficients for nine wavelengths ranging from 410 nm to 715 nm. The values of the absorption and attenuation lengths have been determined for each measurement by averaging the data for depths greater than 2850 m. The results [A. Capone et al., Nucl. Instr. Meth., A487, (2002) 423] of four sets of measurements taken in different seasons are shown in Fig. 1-2 and Fig. 1-3. For comparison light

absorption and attenuation data for optically pure sea water are also shown. At all wavelengths, deep waters at that location have an absorption length compatible with that of pure sea water. There is no evidence of a seasonal dependence of the optical parameters.

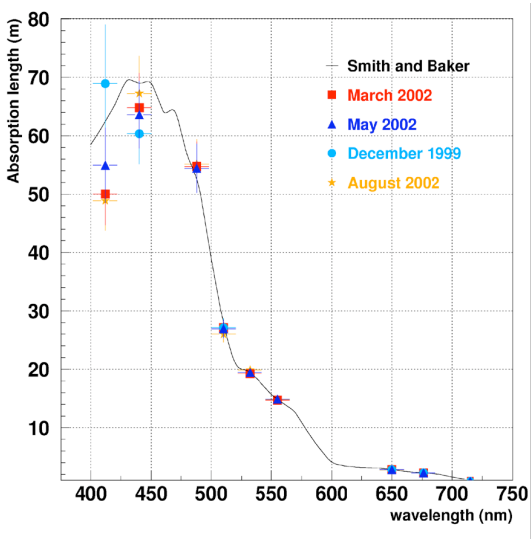

Fig. 1-2 - Average absorption length as a function of wavelength, for four seasons at the Capo Passero site.

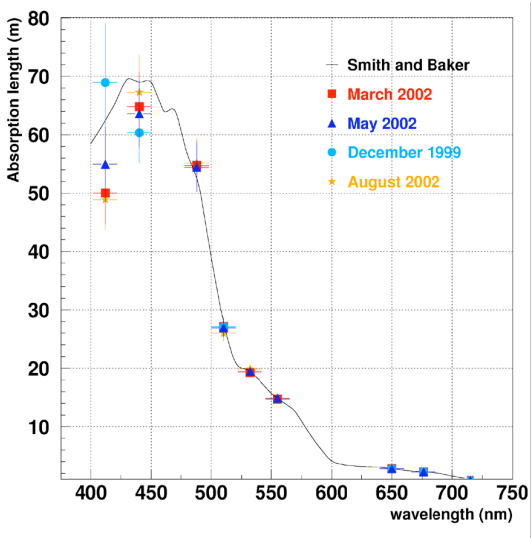

Fig. 1-3 - Average attenuation length as a function of wavelength, for four seasons at the Capo Passero site.

The NESTOR group has developed and operated a detector to measure the "Transmission Length " in deep sea by means of a rigid structure that allow to measure how the distance (R=10, 15, 17, 22 m) between an constant isotropic source and a detector (a photodiode) affects the light intensity. Measurements have been performed at 8 wavelengths (376, 386, 400, 425, 445, 463, 502, 520 nm) in the Ionian sea, at different depths, in Pylos and Capo Passero areas. Table 1-3 shows the results of measurements performed in May 2009 at different depths in Pylos site, Fig. 1-4 shows the results obtained, with the same instrument, in Pylos and Capo

Passero sites.

Transmission Lenght, $L_\beta(\lambda)$ [m], at different depths in Pylos site 4.5D					
Wavelengths	**Depth 2000m**	**Depth 2500m**	**Depth 3000m**	**Depth 3400m**	**Depth 4100m**
375.7	**19.5**	**20.2**	**20.4**	**20.4**	**19.7**
385.7	**22.9**	**24.1**	**24.4**	**24.4**	**23.6**
400.3	**26.8**	**28.3**	**28.8**	**28.8**	**27.6**
425.0	**32.8**	**34.3**	**35.7**	**36.1**	**34.1**
445.4	**36.5**	**39.1**	**40.5**	**41.1**	**39.2**
462.6	**40.2**	**43.6**	**45.1**	**45.6**	**44.1**
501.6	**26.3**	**27.1**	**27.7**	**28.1**	**27.1**
519.5	**19.7**	**20.3**	**20.3**	**20.7**	**20.1**

Table 1-3 - Sea water transmission length as a function of wavelength, measured for several depths at Pylos site.

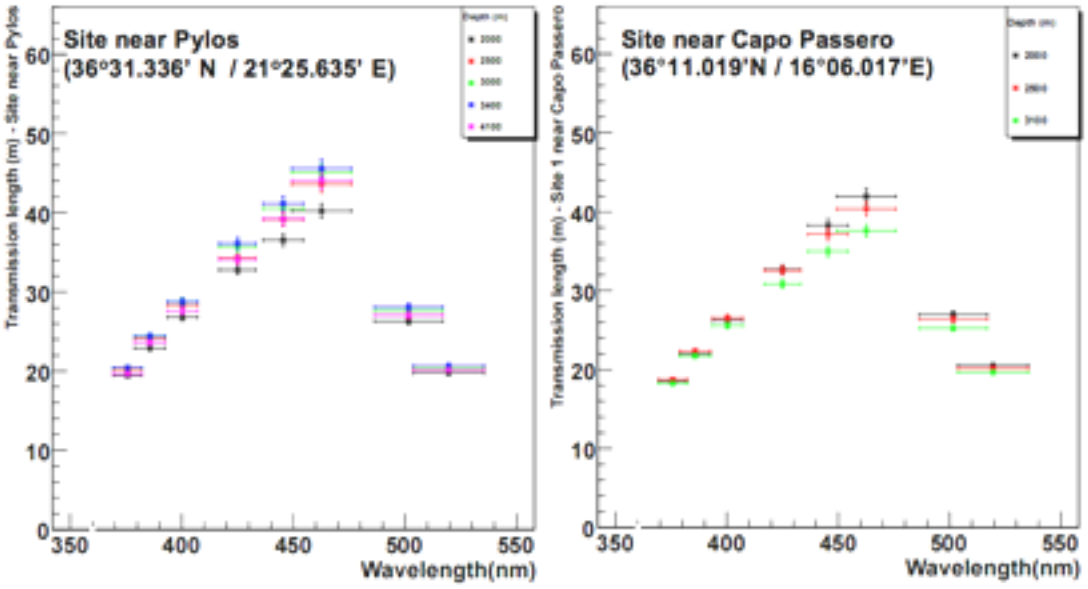

Fig. 1-4 - Transmission length vs λ measured on May 2009 in Pylos and Capo Passero sites.

The absorption length was previously measured at different locations in the Pylos area with an open geometry photometry using a non-collimated light source at a

wavelength of 460 nm. Measurements were made at various depths and for distances between light source and sensor ranging from 7.44 m to 40.37 m. Fig. 1-5 shows the results of the measurements. An absorption length of 55±10 m describes the data satisfactorily [ref. E.G. Anassontzis et al. (NESTOR collaboration), Nucl. Instrum. and Meth., A349 (1994) 242.].

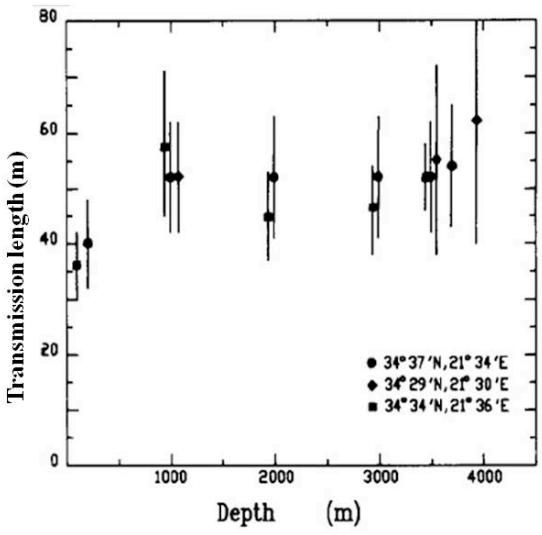

Fig. 1-5 - Absorption length versus depth at 460 nm wavelength in the Pylos area.

1.1.2 Optical Background

The background counting rate in the optical modules of an undersea neutrino detector has two main natural contributions, from the decay of radioactive elements in the water, and from the luminescence produced by organisms (bioluminescence).

Of all the radioactive isotopes present in natural sea water ^{40}K is by far the dominant one. Both ^{40}K decay channels

$$^{40}K \rightarrow {}^{40}Ca + e^- + \bar{\nu}_e \quad (\mathrm{BR} = 89.3\%)$$
$$^{40}K + e^- \rightarrow {}^{40}Ar + \nu_e + \gamma \quad (\mathrm{BR} = 10.7\%)$$

contribute to the production of optical noise. A large fraction of electrons produced in the first reaction is above the threshold for Cherenkov light production. The photon originating in the second reaction has an energy of 1.46 MeV and therefore, through Compton scattering, produces electrons above the threshold for the Cherenkov effect. The intensity of Cherenkov light from ^{40}K radioactive decays depends mostly on the ^{40}K concentration in sea water. Since the salinity in the Mediterranean Sea has small geographical variation, this Cherenkov light intensity is largely independent of the site.

Bioluminescence is ubiquitous in the oceans and in the deep sea there are two sources, the steady glow of bacteria and flashes produced by animals. These can

give rise to an optical background several orders of magnitude more intense than the one due to ^{40}K. Relatively little is known about bioluminescence at great depth. The typical spectrum of bioluminescence light is centred around 470-480 nm [ref. P. J. Henning, Ed., Bioluminescence in action. London, U.K.: Academic Press, 1998, E. A. Widder, ref. I. M. Latz, and J. F. Case, Biol. Bull., 165(1983)791.], the wavelength of maximal transparency of water, which is of greatest interest for undersea neutrino telescopes. The distribution of luminescent organisms in the deep-sea varies with location, depth and time but there is a general pattern of decrease in abundance with depth. The Istituto Sperimentale Talassografico di Messina (CNR), has cultured bacteria from samples of water taken from near the Capo Passero site in 2000 and has detected no luminescent bacteria cultivable at atmospheric pressure from samples taken deeper than 2500 m (see Fig. 1-6) [ref. M. Ambriola et al. (NEMO collaboration), http://nemoweb.lns.infn.it/sites/SiteReport/NEMO-Site-Report.pdf.].

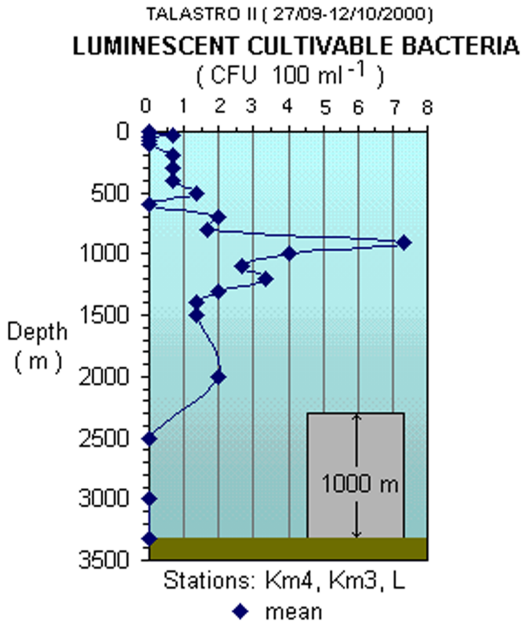

Fig. 1-6 - Amount of luminescent cultivable bacteria as a function of depth, measured at Capo Passero site.

Presence of bioluminescent animals in the water column surrounding the telescope array can contribute to background signal at photo-detectors. Scientists from the University of Aberdeen have developed an experimental set-up, based on a ICDeep camera (I2CCD (Image Intensified Charge Coupled Device for Deep-sea research) to measure the amount of these animals along the vertical water column. Measurements were made in autumn 2008 and spring 2009, in Pylos and Capo Passero sites, to investigate seasonal changes at each site. The Mediterranean Sea is oligotrophic with low biological productivity so abundance of bioluminescent plankton is generally an order magnitude lower than in the Atlantic Ocean. In order to resolve differences between the two sides of the Ionian Sea, the ICDeep camera had a higher sensitivity setting than the ISIT camera used for previous measurements in the Mediterranean Sea (Craig et al. 2009) resulting in higher abundance values.

Results are shown in Fig. 1-7, it has been found a decrease with depth and an abundance which is significantly lower than that in the Atlantic Ocean at similar depths [ref. Gillibrand et al., Marine Ecology Progress Series, 341(2007)37., ref. I.G. Priede et al., submitted to Deep Sea Reseach, part I.]. At a depth bigger than 2500m the amount of this optical background is anyhow negligible for both sides.

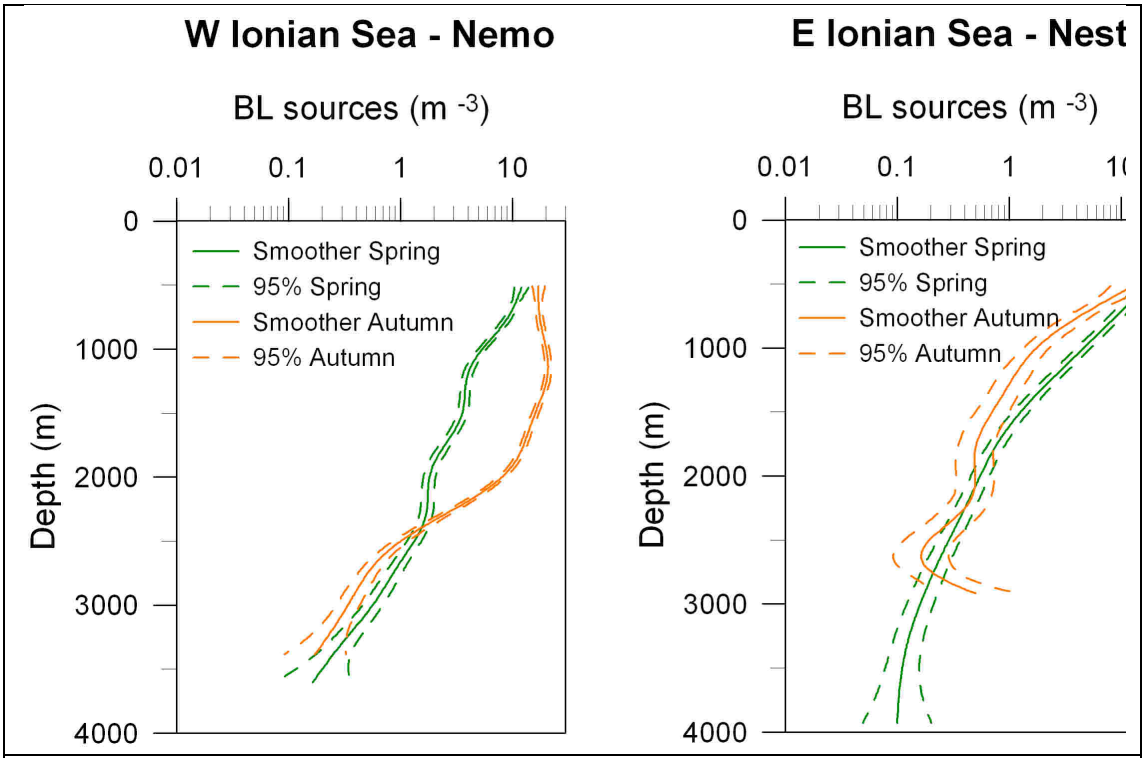

Fig. 1-7 - Abundance of bioluminescent animals per cubic meter of sea water as a function of depths measured in different seasons in the Capo Passero and Pylos sites..

Radioactivity Probe

The constant source of optical background is due to ^{40}K radioactive nuclei decay.

Direct information on the ^{40}K concentration may help in understanding temporal variations of the optical background. The activity of ^{40}K in the Mediterranean Sea is generally assumed to be 13 Bq/l.

A measurement of the actual activity, if different from the expected one, can help to explain variations of the background light.

For this reason a probe capable of measuring the spectrum of -rays from radioactive decays in deep-sea water has been developed. The sensor, which uses a NaI(Tl) crystal, can be used to measure the concentration of the various radio-nuclides occurring in sea water. The instrument was completed in October 2007 (see Fig. 1-8), calibrated in laboratory with radioactive sources and deployed in deep sea, in Capo Passero site for six months (November 2008-May 2009). Over this period the contribution of gamma from ^{40}K has been monitored: preliminary results (Fig. 1-9)

indicate an observed activity compatible with the one expected (about 12 Bq/kg) from the amount of ^{40}K dissolved in sea water.

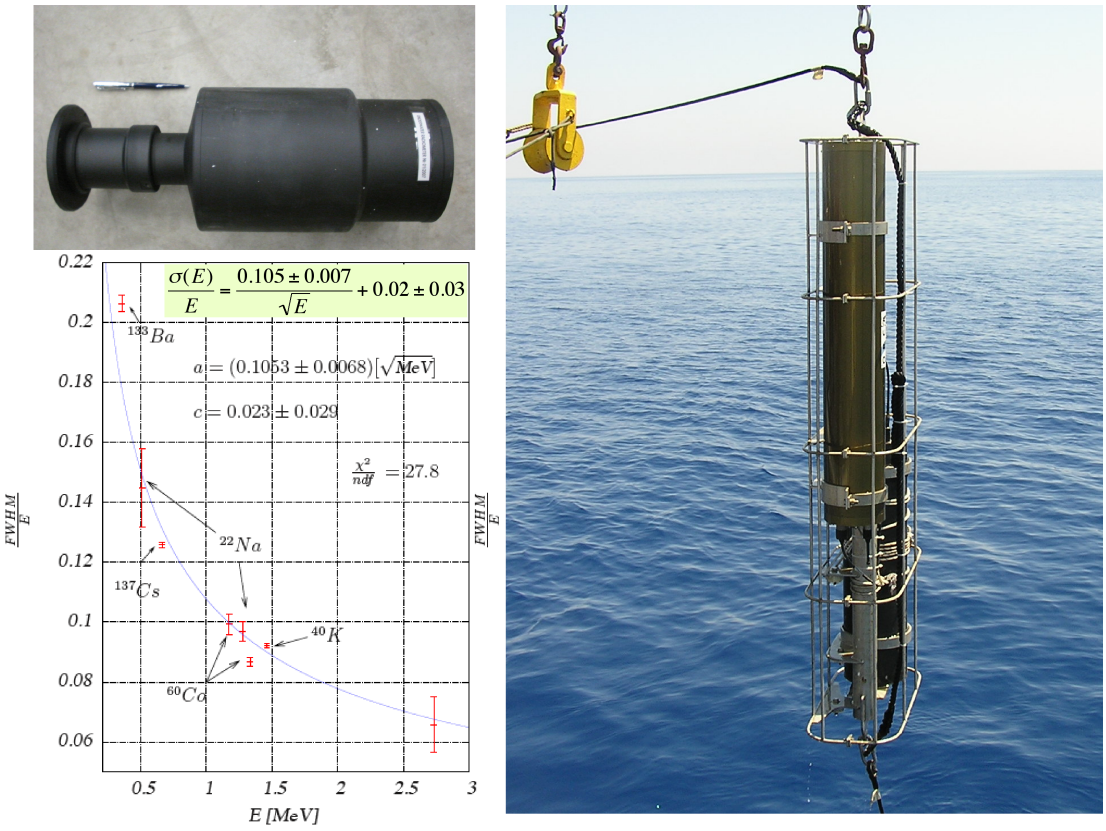

Fig. 1-8 - The gamma spectrometer developed for gamma activity measurements in deep sea. On top left the instrument, below the result of calibration obtained with radioactive sources, on the right the instrument as part of the mooring operated for six months in Capo Passero site.

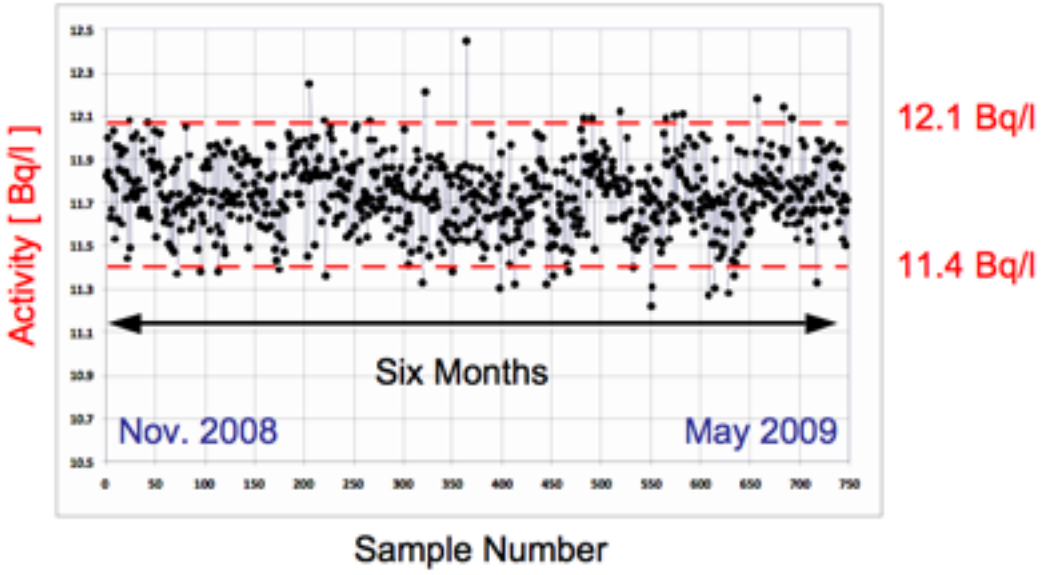

Fig. 1-9 - ^{40}K activity in gamma, as a function of time, measured in Capo Passero site, during six months of deployment

Direct optical Background Measurements

Before detector construction, the ANTARES Collaboration performed a series of in situ measurements of the background light in the Toulon site using 8 inch photomultiplier tubes on autonomous device systems [ref. P. Amram et al. (ANTARES Collaboration), Astroparticle Physics, 13 (2000) 127.]. Two contributions to the optical background were observed: a continuous base rate ("baseline") of a few tens of kHz, varying slowly on time scales of a few hours, and sharp peaks lasting a few seconds and rising to tens of MHz (“bursts”).

A typical time stream of data, acquired in April 2005 [ref. J.A. Aguilar et al. (ANTARES Collaboration), Astroparticle Physics, 26(2006)314.], is shown in Fig. 1-10. A mean counting rate of a single Optical Module during 4 years time is shown in Fig. 1-11. Counting rates were acquired with a threshold of 0.3 photoelectrons. The two components of optical background described above are clearly visible. Bursts observed in the counting rates are probably due to the passage of light emitting animals close to the detector.

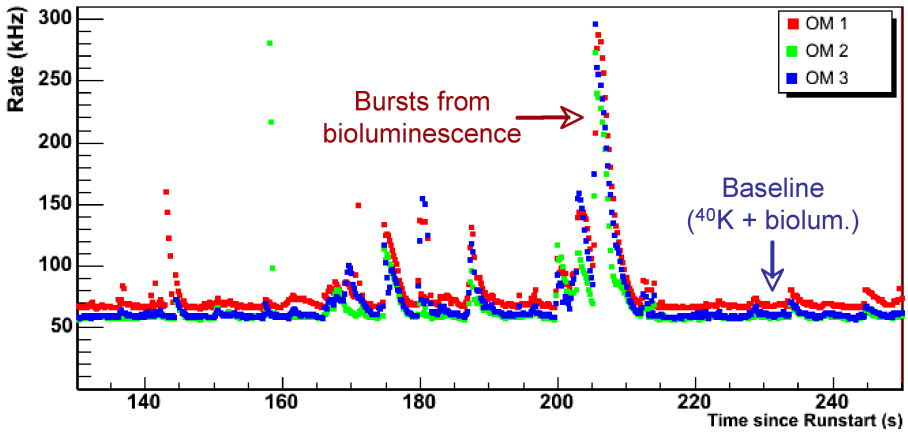

Fig. 1-10 - Typical example of counting rate in three optical modules of an ANTARES line storey. The three colours indicate the individual rates of each of the OM with the small different in the base line counting rate being due to slight differences in detector efficiencies.

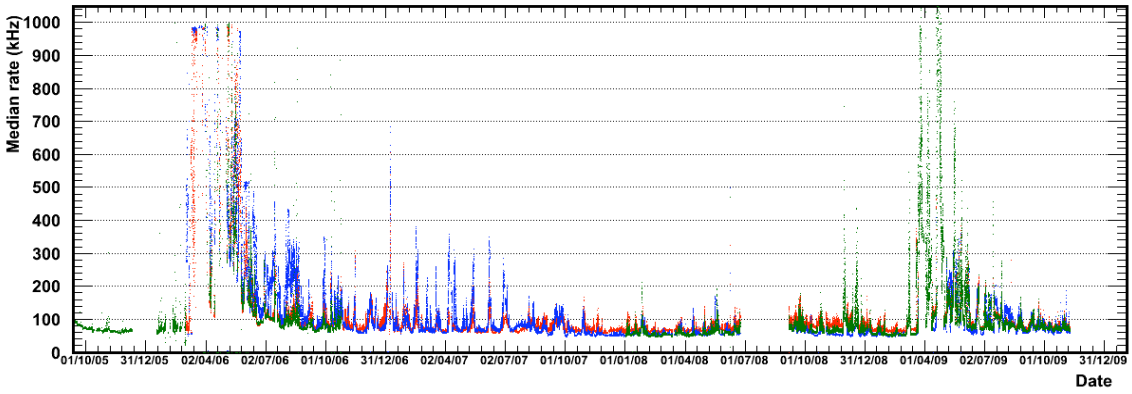

Fig. 1-11 - Mean counting rate in a single OM recorded on the ANTARES site during a period of 4 years between May 2005 and June 2009. The data are from difference OMs in different lines according to the colour code in the legend.

The baseline component is neither correlated with the sea current, nor with the burst frequency; however, long-term variations of the baseline were observed with the ANTARES detector. Periods of high burst activity are not correlated with variations of the baseline component, suggesting that each of the two contributions is caused by a different population. Moreover, a strong correlation is observed between burst activity and the current velocity [ref. M. Naumann-Godó, Nucl. Phys., B (Proc. Suppl.) 172 (2007) 36], as shown in Fig. 1-12.

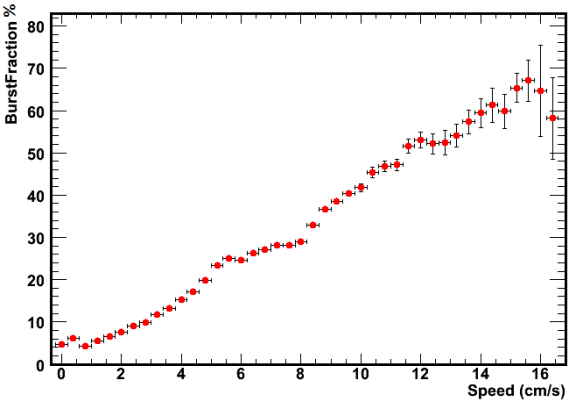

Fig. 1-12 - Correlation between the burst fraction and the sea water current velocity. The burst fraction is the fraction of time with count rates exceeding 120% of the baseline rate. Data sample has been collected from summer 2005 to summer 2006 in Toulon site.

Data in Capo Passero were collected by means of two different setups. One, built by the NEMO Collaboration, consisted of two 8 inch photomultipliers and the associated electronics, the second, built by the ANTARES Collaboration, used an optical module containing a 10 inch photomultiplier. The two devices have been used to collect data separately, but also together in order to assess systematic uncertainties. Fig. 1-13 shows the photomultiplier rate as a function of time, as obtained with the NEMO setup [ref. M. Ambriola et al. (NEMO collaboration), http://nemoweb.lns.infn.it/sites/SiteReport/NEMO-Site-Report.pdf.] using a threshold equivalent to 0.33 photoelectrons.

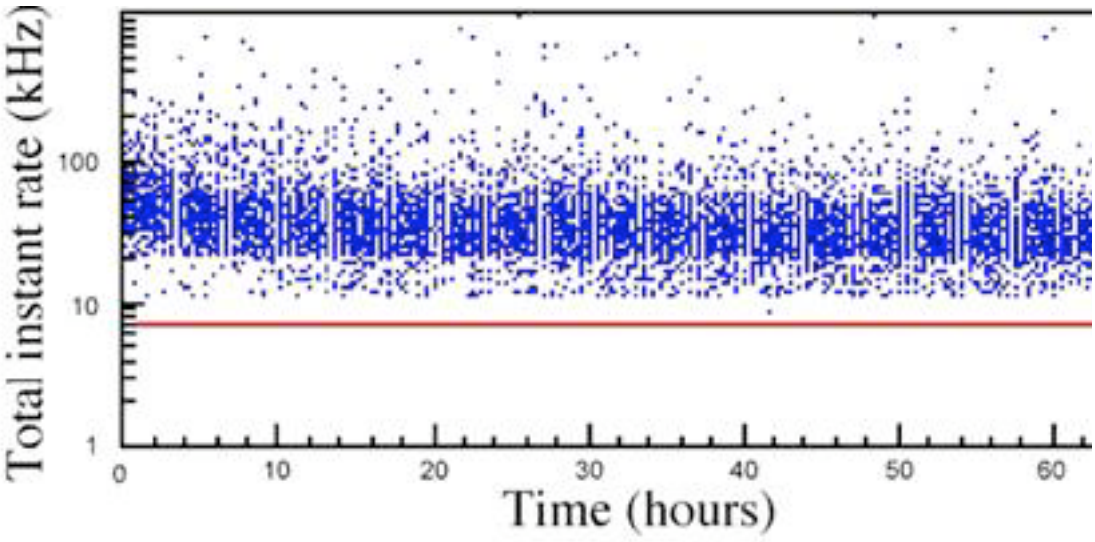

Fig. 1-13 - Photomultiplier count rate, as function of time, for data collected at the Capo Passero site. The red line indicates the dark current count rate.

After subtracting the dark count rate of 7 kHz a counting rate of 28.4 ± 2.5 kHz is obtained. This background is rather constant and shows only rare bioluminescence bursts. From this rate, taking into account the properties of the optical module and the photomultiplier, an isotropic photon flux of 360 ± 40 $cm^{-2}s^{-1}$ in the wavelength range of sensitivity of a bi-alkali photocathode is found. This flux is consistent with the expectation from just the 40K decays.

Also in the Pylos area the optical noise has been measured on several occasions and with different devices. A number of free-drop experiments have been performed since 1996, at a depth of 4000 m, with an apparatus composed of two optical modules. The NESTOR floor deployed in 2003 was also used to study the optical background [ref. A. G. Tsirigotis, Ph.D.Thesis, Hellenic Open University, Patras, Greece, 2004.]. A data sample of 100 s duration is shown in Fig. 1-14 [ref. E.G. Anassontzis et al., Nuclear Physics, B (Proc. Suppl.) 151 (2006) 279]. From the analysis of the full data sample it is concluded that bioluminescence occurs during 1.1% ± 0.1% of the time.

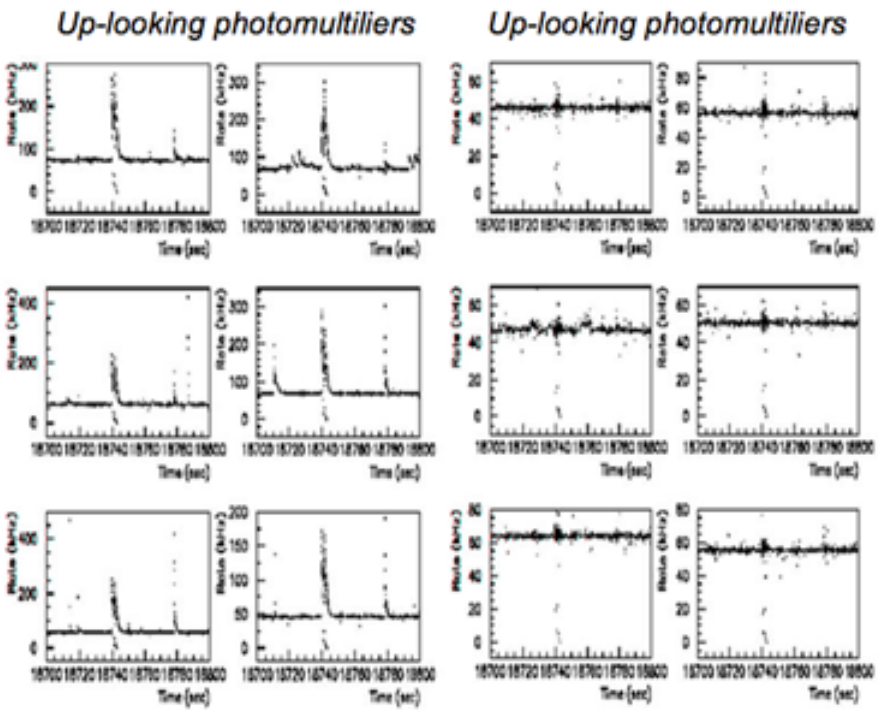

Fig. 1-14 - Count rates of the 12 photomultipliers of the NESTOR floor; bioluminescence bursts are clearly seen.

1.2 Deep-Sea Currents

Deep sea currents were monitored at the three sites for long time periods.

At the Toulon site measurements were performed during the exploratory phase using autonomous mooring lines. Since the deployment and the connection to the shore of the instrumentation line (2005), the measurements are continuously performed in real-time.

As an example the plot in Fig. 1-15 illustrates the time dependence of the current velocity since September 2005, while Fig. 1-16 shows the distribution of the current velocity measured in the same period. From these data we learn that during 75% of the time, the current, in ANTARES site, was below 8 cm s^{-1}.

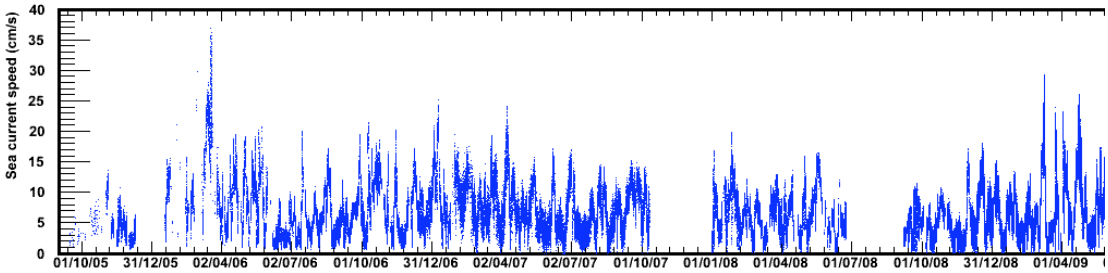

Fig. 1-15 - Measurements of sea current speed, in the period September 2005 - October 2009, in the Toulon site. The data is mainly from the ADCPs on the instrumentation lines but between June and December 2007 is from the Aquadopp device on line 5 of the neutrino telescope.

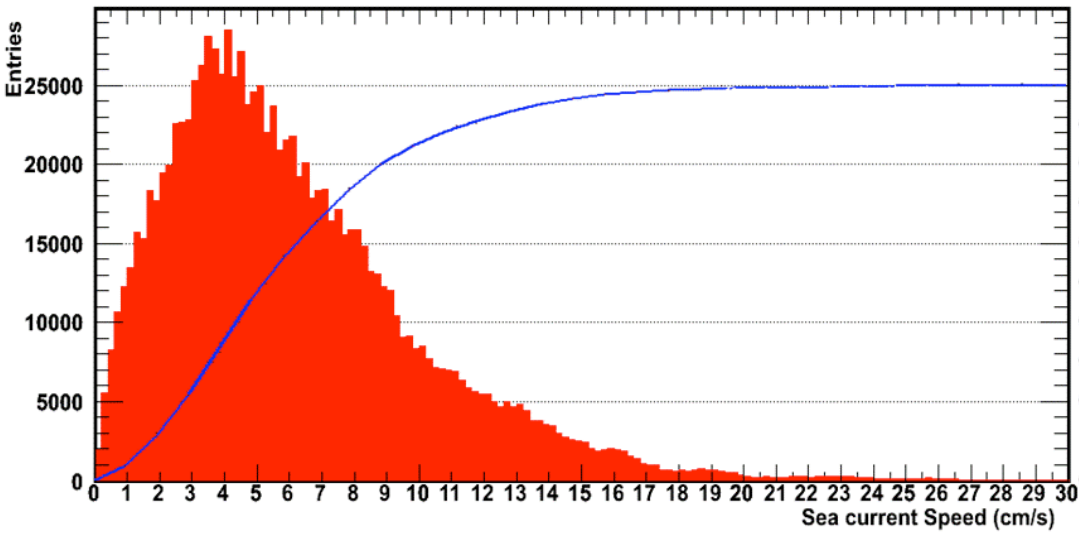

Fig. 1-16 - Distribution of the current velocity measured, in ANTARES site, in the period September 2005 - October 2009. The red line represents the integrated content of the histogram and helps to conclude that during 75% of the time, the current was below 8 cm s^{-1}.

Measurements of deep-sea currents in the region of Capo Passero have been performed with current-meter moorings. Current intensity and direction have been monitored almost continuously since 1998, in a range up to 500 meters above the seabed (see Fig. 1-17). A complete analysis of the current meter data for the period July 1998 – December 1999 has been reported [ref. L. Ursella, NEMO Internal Note http://nemoweb.lns.infn.it/sites/SiteReport/NEMO_Annex4-Report-Currents.pdf, 2002.].

Further observations were carried out from August 1999 to August 2002 and from May 2007 to May 2009. All acquired data agree in showing no significant depth dependence of the deep sea current. The same current maintained an almost stable direction (Fig. 1-17). The intensity evidenced a slow increase during the last period, moving from a mean value of 3.2±1.8 cm/s to 4.3±2.3 cm/s. Spanning the observations along 10 years, it may be related to the inter-annual variability of the deep Ionian circulation. While the highest measured current intensity was 13.5 cm/s, the 80% of the observed values were always lower then 5 cm/s (see Fig. 1-18).

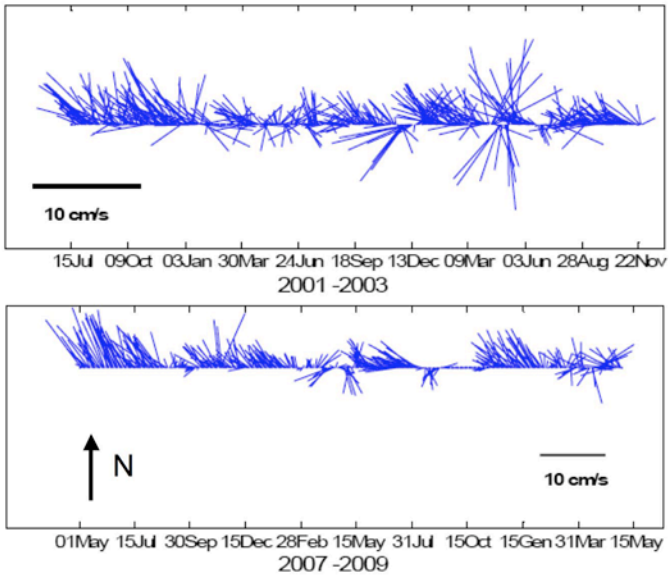

Fig. 1-17 - Deep sea water current speed intensity and direction from measurements performed in the period 2001-2004 and 2007- 2009, in Capo Passero site.

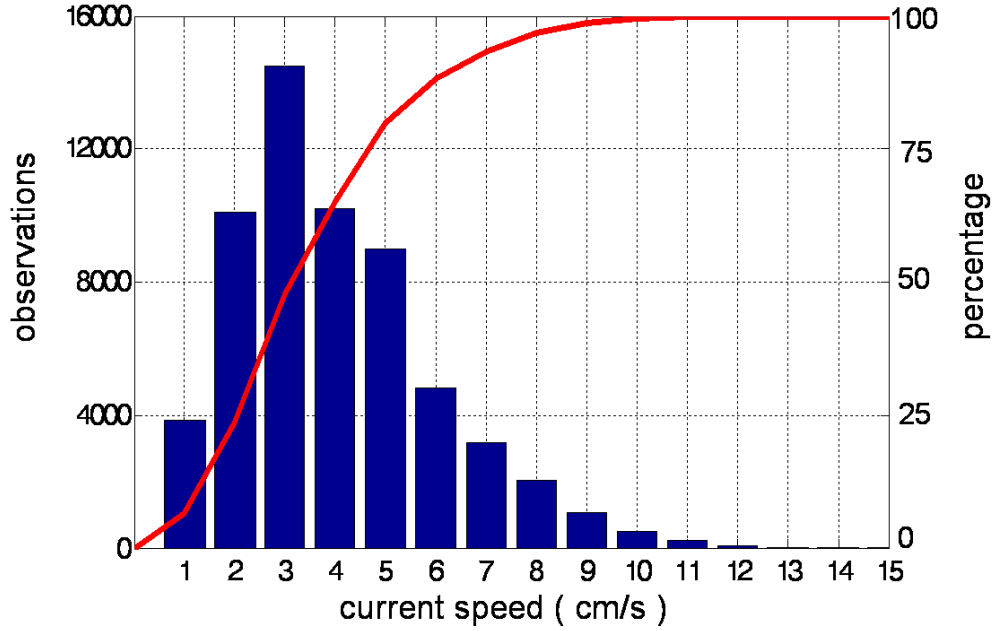

Fig. 1-18 - Distribution of current speed at NEMO site, comprehensive of observation periods 2001-2004 and 2007-2009. Red line represents the percentage of the cumulative distribution.

At the Pylos site the deep-sea currents have been monitored since 1989 with different moorings and current-meters [ref. T.A. Demidova et al., in Proc. 2nd NESTOR Int. Workshop , 1992, 284., ref. G. Aggouras et al. , Nucl. Instrum. Meth., A567(2006)468.]. The deep currents have low velocities that rarely exceed 6 cm s^{-1}.

In general, as shown in Fig. 1-19, the flow at the Pylos site of 4500 m depth is northward and 90% of the time is below 4 cm s^{-1}, and at the 5200 m deep site is southward but substantially weaker, with 95% of the time the current speed being below the measurement threshold.

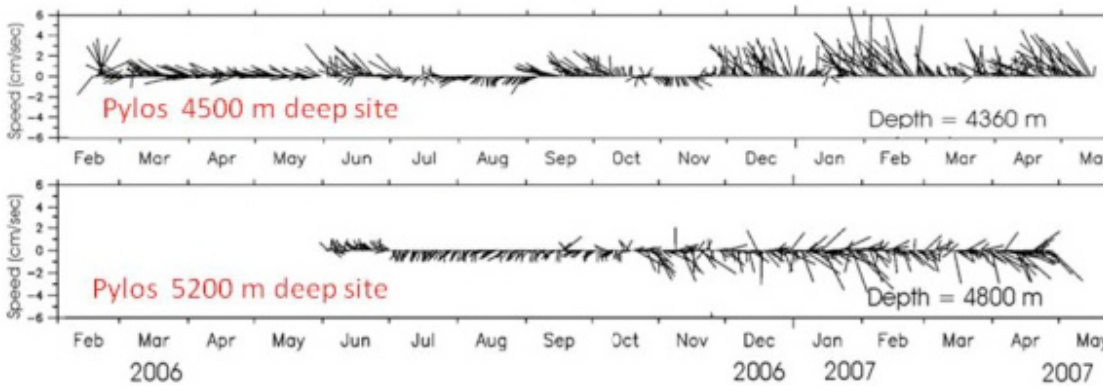

Fig. 1-19 - Sea water current measurements in the Pylos area. Measurements have been taken every 8 hours, North is towards the top.

1.3 Sedimentation

The rate of sedimentation at three areas has been obtained from sediment traps deployed at the sites in different years. The highest mass flux during the late winter and spring were recorded at the Capo Passero site [ref. M. Ambriola et al. (NEMO collaboration), http://nemoweb.lns.infn.it/sites/SiteReport/NEMO-Site-Report.pdf.], and the Toulon site [ref. P. Amram et al. (ANTARES Collaboration), Astroparticle Physics, 19 (2003) 253] showed the highest mass flux values during the autumn and early winter period (see Fig. 1-20).

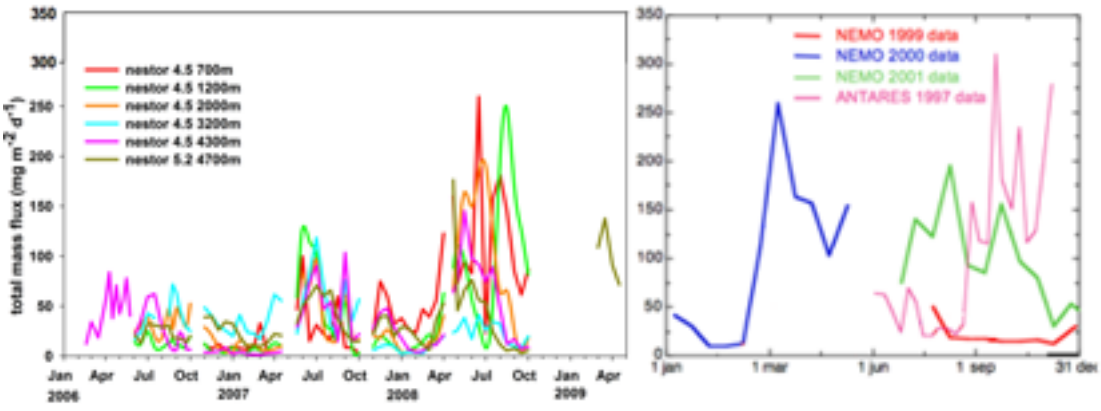

Fig. 1-20 - Downward total mass fluxes from the three areas.

Optical Sedimentation Measuring System

Sedimentation on Optical Modules have been studied by means of special devices capable to measure, as a function of time, the glass sphere variation of transparency

(fouling) as a function of the angle to the vertical direction.

Several autonomous instrumentation set-up have been developed and operated By ANTARES (ref. P. Amram et al., Astropart.Phys. 19 (2003) 253-267), NEMO and NESTOR [ref. E.G. Anassontzis et al. (NESTOR collaboration), NESTOR NOTE.160.2007, 2007] Collaboration.

As an example we show, in Fig. 1-21 the schematics of the devise (LIMS) built by NESTOR Collaboration.

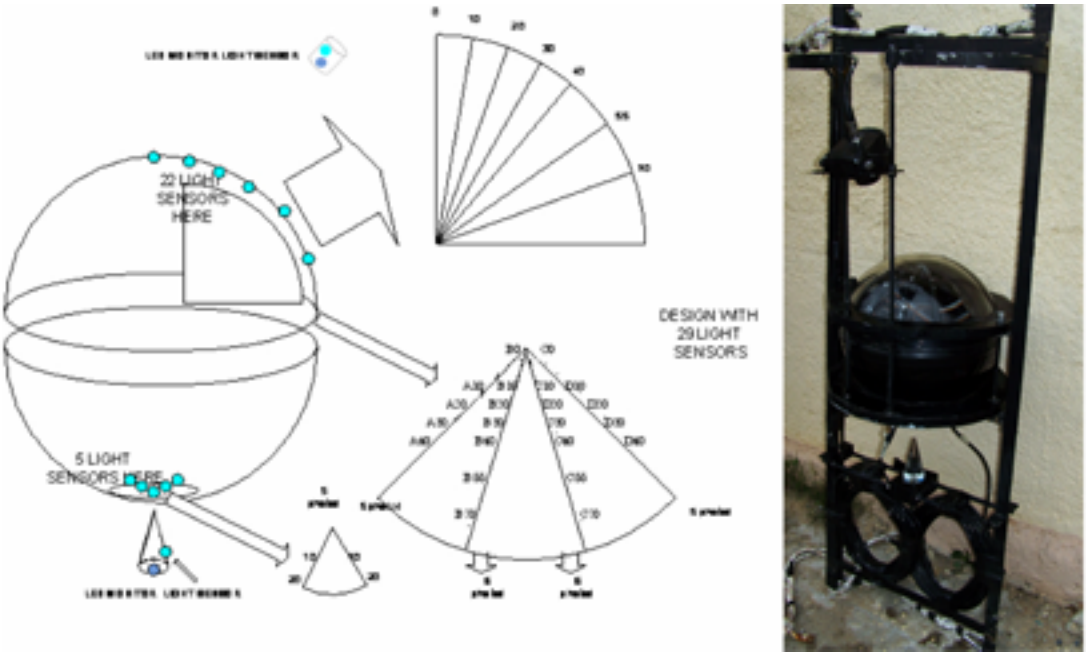

Fig. 1-21 - LIMS glass housing and mechanics.

In the 3 sites data have been accumulated for long periods, the resulting samples have been analysed to study variation of transparency of glass surfaces and the correlation of this variation with underwater currents.

Results from measurements in Toulon site are shown in Fig. 1-22: a general trend of decreasing fouling with increasing zenith angle on the glass sphere. We observed a very rapid decrease (within a few days) in the transmission at the top of the sphere ($\theta = 0$), but less change at larger zenith angles. The transmission is seen to recover from time to time in partial correlation with an increase in the measured water current velocity (bottom of figure). From these data ANTARES derived that the loss of light transmission for a vertical glass surface is estimated to be less than 2% after one year.

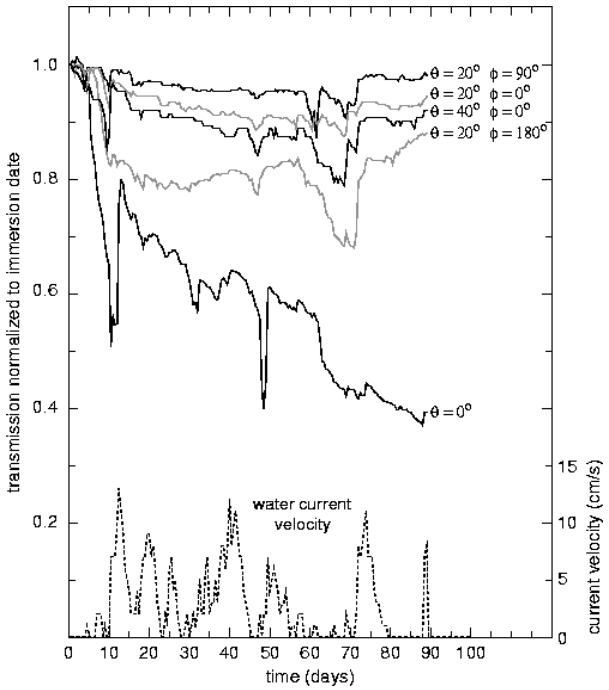

Fig. 1-22 - Light transmission variation on optical glasses in Toulon site, as a function of time from the first immersion day. The measurements for each of the 5 photodiodes are normalized to unity at immersion, on January 25, 1997. Curves are labelled according to the photodiode coordinates on the glass sphere surface (zenith, φ, and azimuthal, θ, angles). The current velocity is indicated at the bottom of the figure.

Analogous measurements have been performed, for a 18 months long period, in Capo Passero site at about 3300m depth. Fig. 1-23 shows the effect of the angle (to respect to the horizontal direction) on the fouling. Also in this case below the horizontal diameter of the sphere the effect of fouling on transparency variation is less than 2% for one year exposure.

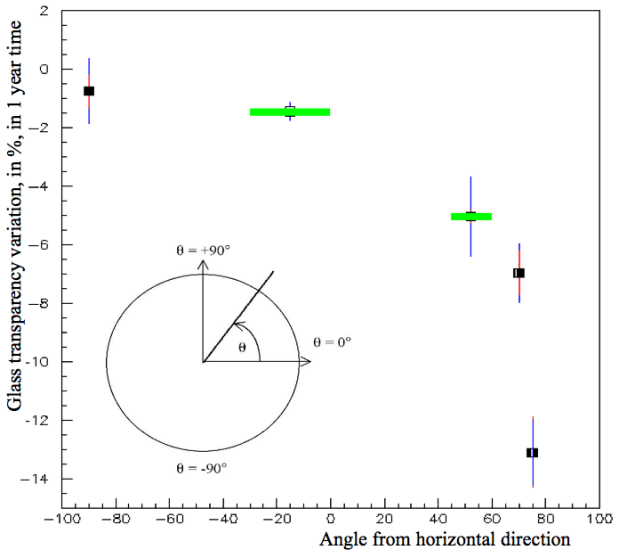

Fig. 1-23 - Effect of fouling on glass spheres in Capo Passer site, as a function of the angle from the horizontal direction. Data have been collected over 18 months, the variation of transparency here is indicated in % and for one year immersion.

The LIMS instrument was deployed for long periods in Pylos site and allowed to

compare (Fig. 1-24) the results obtained with the variation of transparency of the glass surfaces with the results from sediment traps moored in the same area and during the same period. The results obtained seem to be consistent with the ones reported by ANTARES and NEMO.

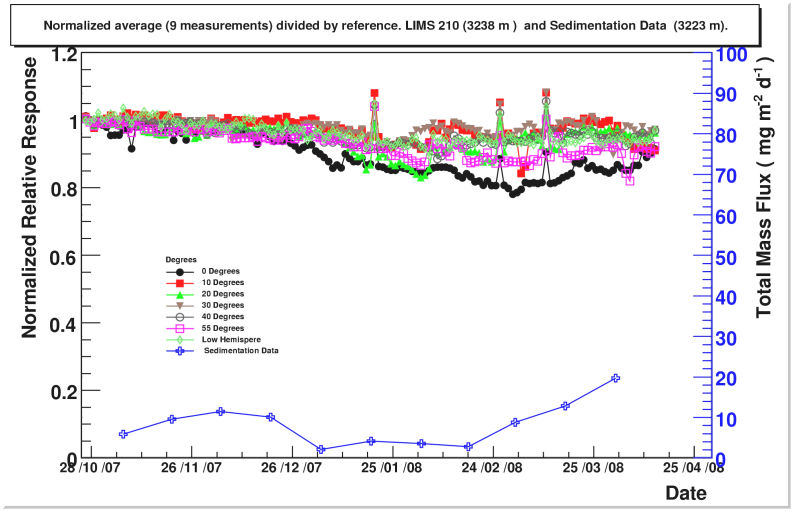

Fig. 1-24 - Variation of transparency on a glass sphere, due to sedimentation, as a function of zenith angle, measured in Pylos area at 3200m depths. The optical measurements performed with LIMS are compared with sedimentation fluxes measured by means of traps, in the same area and in the same period.

2. Study of the Telescope Deep Sea Network

2.1 General description

The detector layout presented in this document is the result of a configuration optimisation performed with a Monte Carlo simulation described elsewhere in this document. The geometry parameters that have been optimised are: the spacing between detection units; the spacing between storeys; the bar length of the storey as well as the number and orientation of the PMTs in the storey.

We assume here that the Detection Units (DU, already described in this document) will be, schematically, arranged on the seabed in a hexagonal form with 180m spacing between DUs (Fig. 2.25). For reasons connected to deployment and connection operations a wider distance between the towers located on the central axes has been also envisaged.

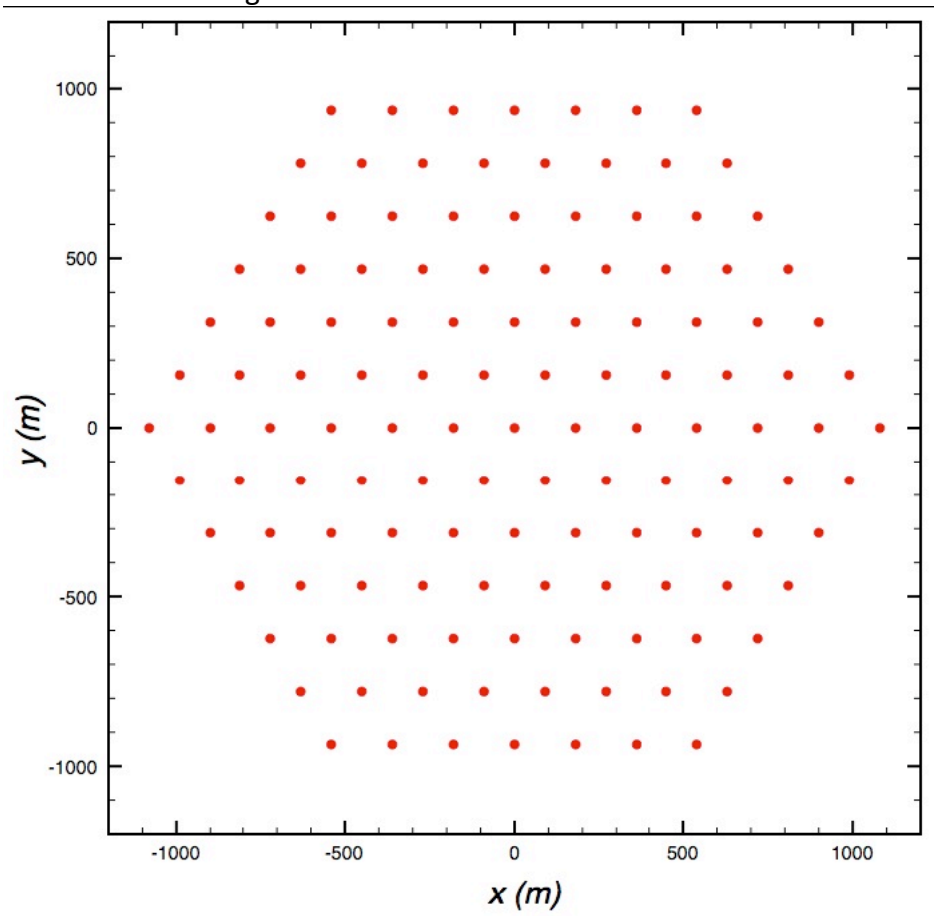

Fig. 2.25 – Seafloor layout for the 127 DUs detector.

A Main Electro-Optical Cable (MEOC) will provide the connection of the detector to shore for power feeding and data bidirectional transmission. A hierarchy of Primary (PJB) and Secondary (SJB) Junction Boxes will allow the distribution of services to the individual DUs.

In deep sea, the mechanical structures holding the optical modules move under the effect of currents, thus their positions must be continuously monitored using an acoustic positioning system (acoustic beacons and hydrophones).

Two kind of solutions for the data and power distribution layout have been proposed, one is based on a "star" like layout of cables (see Fig. 2.26), the other distribution is characterized by a "ring" geometry" (see Fig. 2.38). The two solutions have not been developed at the same level of details so the first one will be extensively described, the second one will be mentioned at the end of the chapter as one of the study going on.

2.1.1 Power and Fiber Optical data connection with a "star" layout

The connection of the on-shore laboratory and the telescope is provided by a system of optical fiber carried by the MEOC and distributed the DUs by a network that involves the PJB and the SJB.
Here we start with the description of the "star" like layout.
Fig. 2.26 shows the scheme of the power and fibre optic distribution.

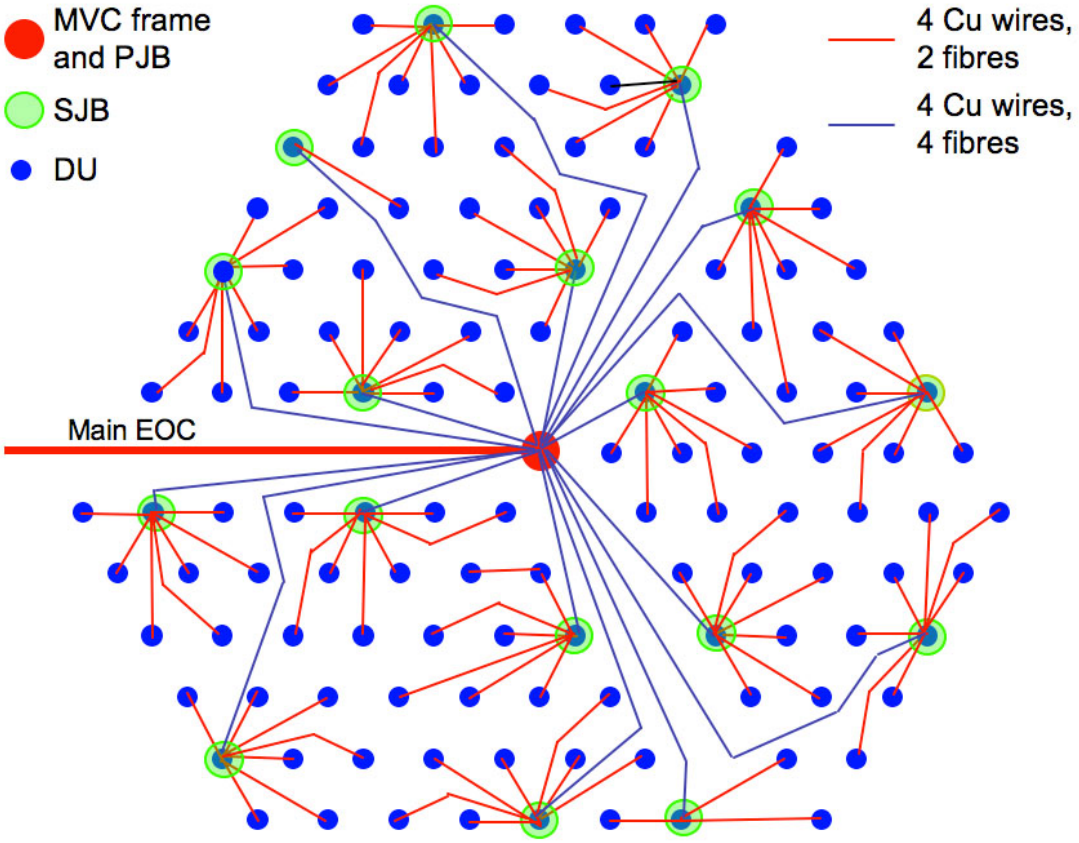

Fig. 2.26 - Scheme of power and fibre optic distribution.

The scheme has been defined taking into account limitations dictated by the cables and PJB, SJBs and DUs deployment and interconnection operations. Three "corridors", ~300m wide, are realized separating the whole detector into three parts such to allow for the laying of the MEOC and the passage of an ROV for deployment, connection and maintenance operations. The PJB (and the MVCs) is located at the centre of the detector. All the SJBs are located either along the "corridors" or externally to the detector layout. Each SJB is connected to eight DUs (only one is

connected to 4 DUs and 1 to only 2 DUs) in agreement with the requirement of the solution chosen for data transmission on optical fibres. The cables (from PJB to SJBs and from SJBs to DUs) are never superimposed; the cable lengths are as short as possible mainly to reduce the power dissipation (the length of cables from PJB to SJBs are less than 1.5 km, from SJB to DUs are less than 400m).

2.1.2 Power Distribution

The power feed and distribution system is based both on the experience gained in ANTARES and NEMO. It takes into account current market availability and deployment issues.

The main design requirements considered are:

- 127 DUs;
- power load of the individual DUs up to 300 W.
- distance to shore of the deep-sea installation up to 100 km;

The total power load, off-shore, for the 127 DUs amounts to about 38 kW.

The power consumption foreseen for the Associated Science equipments will amount to about 10 kW, so the total power that will be required off-shore is of the order of 48 kW.

It will be described later that, including all power losses, the on-shore power needs will amounts to less than 70 kW.

The power feed system is in DC and is based on a 10 kV / 375 V DC, 10 kW Medium Voltage Converter (MVC) like the one developed by Alcatel for the NEMO project, based on a design developed by JPL-NASA for the NEPTUNE project (ref. B. Howe et al. IEEE J. Oceans Eng. 27 (2002) 267 and http://www.neptune.washington.edu)

The MVCs needed to feed the required power load are located in a frame placed close to the Primary Junction Box. The power distribution to the DUs is in low voltage (375 V). The optimization of this solution requires an opportune location of the PJB, i.e. at the centre of the detector layout, in order to avoid the use of long and/or large section cables from PJB to SJBs.

The electrical power system is divided into the following subsystems:

- a Transmission System, going from shore to the deep-sea site, including the on-shore power supply, the MEOC and its terminations;
- a Distribution System, going from the off-shore MEOC termination to the DU base;

The distribution system has been designed in such a way to guarantee a voltage drop, and Joule losses, (from PJB to DU) less than 4%;

To follow this requirement the cables should have the following characteristics:

- PJB-SJBs cable: 4 Cu conductors, with 13 mm^2 cross section, 600 V nominal voltage and a maximum length of 1500 m;

- SJB-DUs cable: 4 Cu conductors with 2,5 mm^2 cross section, 600V nominal voltage and a maximum length of 400 m.

The power flow from on-shore to off-shore for the 127 DU apparatus, and the Associated Science equipment, is summarized in Table 2-1 and in Fig. 2.27.

Number of DUs	127
Power load per DU	300 W
Power load per 127 DU	38.1 kW
Interconnecting Cables Joule losses (375 V DC) < 4%	1.6 kW
Interconnecting Cables voltage drops	< 4%
Associated Science power load	10 kW
MVC losses (η = 80%)	12.4 kW
Total power off-shore	62.1 kW
Main cable Joule losses	6.7 kW
Total power losses	30 %
Power on-shore	68.8 kW

Table 2-1 - Power budget for the 127 DU detector.

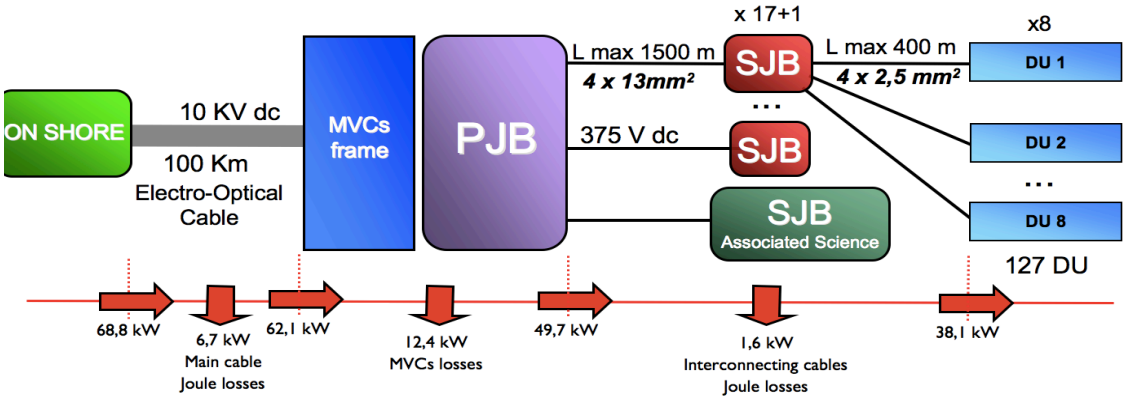

Fig. 2.27 – Power flow block diagram.

2.1.3 Power transmission system

The Transmission System from shore to the detector deep-sea site is in DC with sea return. Its main components are (Fig. 2.28):

- an on-shore 70 kW Power Feed Equipment with a 400 V AC 3-phase input voltage, a 10 kV DC output voltage and 7 A output current;
- a 10 kV DC MEOC with a single conductor and sea return;
- two earth terminations, the anode on-shore and the cathode off-shore.

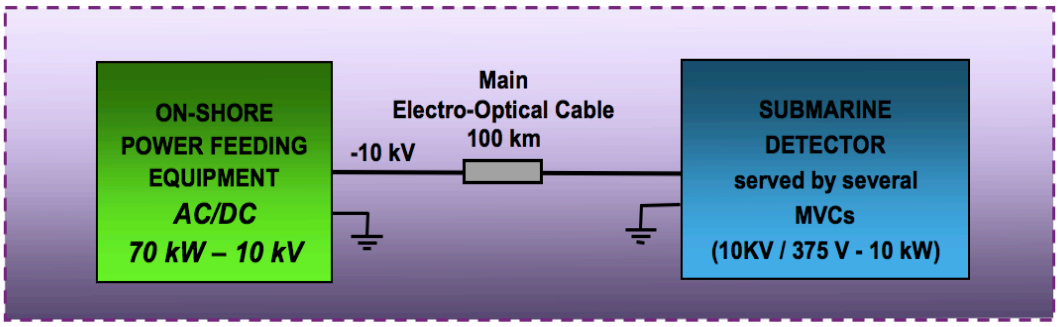

Fig. 2.28 – Block diagram of the power transmission system

The power distribution system goes from the off-shore MEOC termination to each DU base. The voltage conversion, from the transmission value of 10 kV to the distribution one of 375 V, is done by means of Medium Voltage Converters. We envisage to use 7 MVCs, one for redundancy, of the type developed by ALCATEL for the NEMO project, to accommodate the ~60 kW power load (included losses) located into a frame positioned close to the PJB.

The Primary Distribution System includes:

- 1 Primary Junction Box;
- 17 Secondary Junction Boxes (15 SJBs are connected such that each one serves 8 DUs, 1 SJB serves 4 DU)
- a 18th SJB is dedicated to the Associated Science equipment, providing a 10kW maximum power feed.

A schematic example of a layout that optimizes the cable lengths is shown in Fig. 2.26. The system is characterized by the following maximum distances:

- PJB - SJB: 1500 m;
- SJB - DU: 400 m;

The power distribution (Fig. 2.29) is a 375 V DC star configuration from the PJB to the SJBs and from each SJB to the 8 DUs.

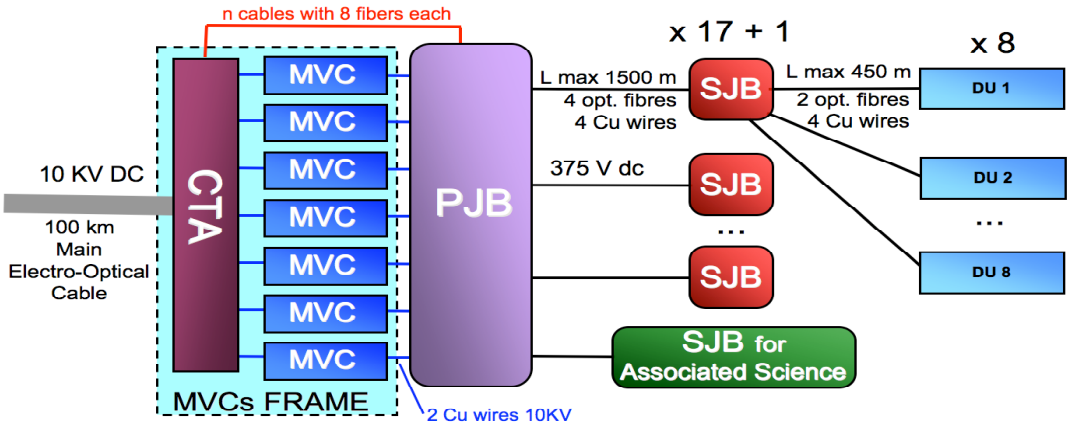

Fig. 2.29 – Block diagram of the Primary Distribution System.

2.1.4 Cables and Connectors

A Main Electro-Optical Cable (MEOC) will provide the connection of the detector to shore for power feeding and data bidirectional transmission. The properties of the MEOC will be more extensively described in Chapter 4.

The MEOC characteristics, according to the power transmission needs previously described in this document are summarized in **Table 2-2**.

Length [km]	100
Type of power to be transmitted	DC, one polarity + sea return
Maximum Voltage [kV]	10
Maximum Current [A]	10
Power Transmission efficiency	95%
Cable resistance [Ω/km]	1
Number of fibres	up to 48

Table 2-2 - Main Electro-Optical Cable characteristics

The MEOC has will be equipped with standard monomode G655 fibres (MFD, LEAF or NZDSF fibres).

One example of MEOC already deployed for deep-sea data and power transmission is the 100 km cable that will operate between the Capo Passero on-shore laboratory and the deep sea site at 3500m depths.

The MEOC will be connected to the MVCs through a Cable Termination Assembly box where conductors and fibres are split. The CU wires exit from the CTA (2 Cu conductors) by means of dry HV penetrators and are connected to the MVCs by means of dry HV connectors (Purely electrical). The fibres exit from the CTA, in groups of 8, with optical penetrators, and go to a Panel equipped with bulkheads ROV operated connectors (purely optical). From this Panel the fibres will be connected to the PJB by means of cables (with only 8 fibres) and purely optical deep-

sea ROV operated connectors. The Panel contains also bulkheads connectors to allow the electrical connection of the 375V MVC outputs and the PJB inputs, using ROV operated deep-sea electrical connectors.

The PJB to SJB and the SJB to DU cables have to be dimensioned according to the power needs and the number of fibres required by the data transmission system.
The interlink cable between the PJB and each SJB has the following characteristics:

- 4 Cu conductors with 13 mm^2 cross section, 600 V nominal voltage
- 2 fibres for each group of 4 DUs connected. This means that the cables that will interconnect the PJB and those SJB that serve 8 DUs will contain 4 fibres.

The interlink cable between each SJB and a DU has the following characteristics:

- 4 Cu conductors with 2.5 mm^2 cross section, 600 V nominal voltage
- 2 fibres

The interlink cables are terminated with hybrid ROV mateable connectors. The sum of conductors and fibres in the interlink cables should be no more than 8 (see Fig. 2.34), this permits to use of hybrid COTS connectors.
This interlink EO cable connects the DU base to the secondary JB. All the designs propose to have, during the deployment, this cable wound on a reel and fixed to the anchor. The cable ends by a wet mate connector of hybrid type or by a pair of such connectors, one electrical and the other optical. The reel as well as the connector is handled by a ROV.

2.1.5 Medium Voltage Converter

At the end of the MEOC there will be a Frame Termination Assembly that will hosts:

- a cable termination assembly to permit to split power and fibre optics,
- a system of Medium Voltage Converters (MVC),
- a Splitting Box with several output wet-mateable connectors.

A MVC has been developed within the activities of the NEMO experiment by ALCATEL: this experience can be the basis of the KM3NeT future hardware.
The converter has an input of up to 10 kV DC and output of 375 VDC/28 A. The measured efficiency is greater than 87% at full load. The converter configuration is 48 Power Converter Building Blocks (PCBB) arranged as matrix of 6 parallel legs with 8 in series in each leg (Fig. 2.30). This arrangement allows for faults within some PCBB's without a failure of the full converter.

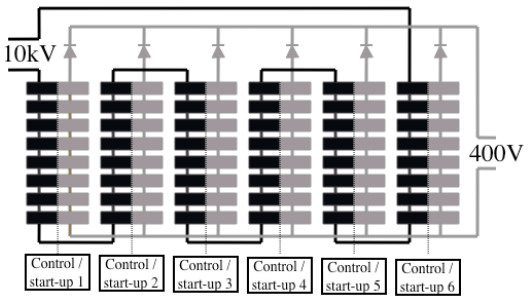

Fig. 2.30 – The DC/DC Medium Voltage Converter layout

The PCBB is a pulse width modulated switching forward converter with an input of 200 V and an output of 50 V at around 200 W. Each block has four MOSFETs, two working as a primary switch and two on the secondary side as a synchronous rectifier. A block diagram of the circuit is shown in Fig. 2.31. The various transformers are able to withstand continuous 10kV operation in a dielectric fluid.

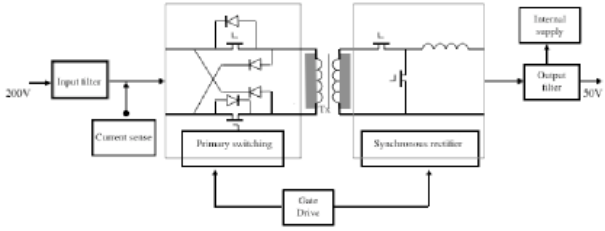

Fig. 2.31 – The DC/DC Medium Voltage Converter PCBB block diagram

The entire power converter is housed in a pressure vessel, Fluorinert® filled to facilitate the cooling and reduce voltage clearances. An entire stack, that include eight PCBB in four boards and a control board it's shown in Fig. 2.32.

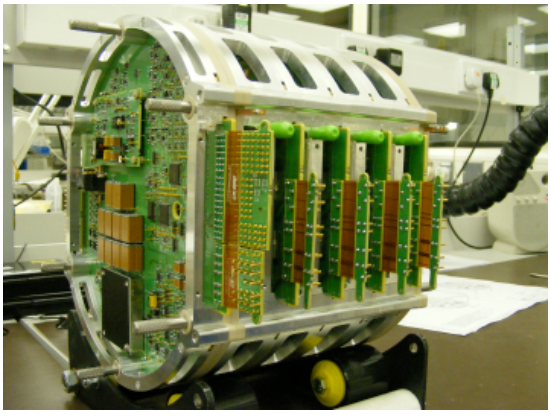

Fig. 2.32 – The DC/DC MVC complete parallel "stack"

Its final arrangement, it's shown in Fig. 2.33.

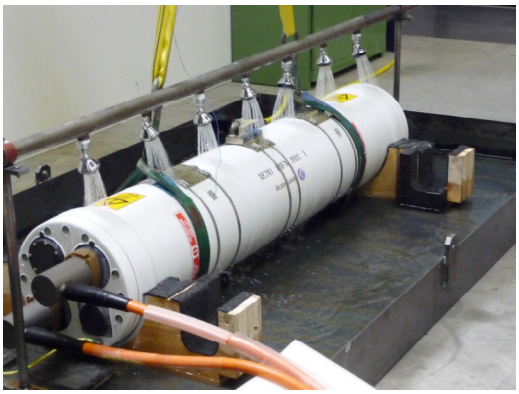

Fig. 2.33 – The Medium Voltage Converter complete assembly

After several years of design, development, assembly and testing, the MVC delivered on September 2009. Several tests have been carried out to verify the functionality and performance of the MVC in particular working conditions: long feeding lines from the 10 kV power supply to the MVC (100 km), long interconnecting cables of the MVC output with the electrical loads and distributed switching DC/DC converters as electrical loads.

The results of the tests were positive as the MVC worked properly without causing any oscillation or instability in the system. The main characteristics of the MVC are showed in Table 2-3.

Input Voltage	5,7 ÷ 10 kV
Output Voltage	375 V
Output current	25 A
Input shut down voltage	5,2 kV
Efficency at 6kV, full load	88,9%
Efficency at 10kV, full load	85,4%
Voltage undershoot at 10kV -10% to 90% step up	40 V
Voltage overshoot at 10kV -90% to 10% step down	43V
Output Ripple Voltage	1,5 Vrms at 100 kHz

Table 2-3 - Medium Voltage Converter characteristics

2.1.6 Junction boxes

The seafloor network will consist of a main electro-optical cable running from the shore to a main junction box in the deep sea and of a network of secondary junction boxes linked by electrooptical cables and connecting to the telescope detection units and the associated sciences nodes. The final design of the network is still under development and may incorporate redundancy to mitigate single point failures.

2.1.7 Primary Junction Box

The block diagram of the Primary Junction Box is shown in Fig. 2.34. Its main functions are:

- to accept the 375 V power from the Medium Voltage Converters (MVC). Several MVC units will be used to accommodate the total power needs;
- to distribute power to the Secondary Junction Boxes (SJB). The input power lines from MVCs will be connected inside the PJB in such a way that a SJB can be feed by more than one MVC providing the needed redundancy (Fig. 2.34);
- to monitor and control all the electrical parameters of the outputs lines;
- to remotely actuate the relays that connect the SJB to the MVC system, to switch on and off the feed lines during normal operation and to isolate a faulty line;
- to communicate to shore by means of optical fibres.

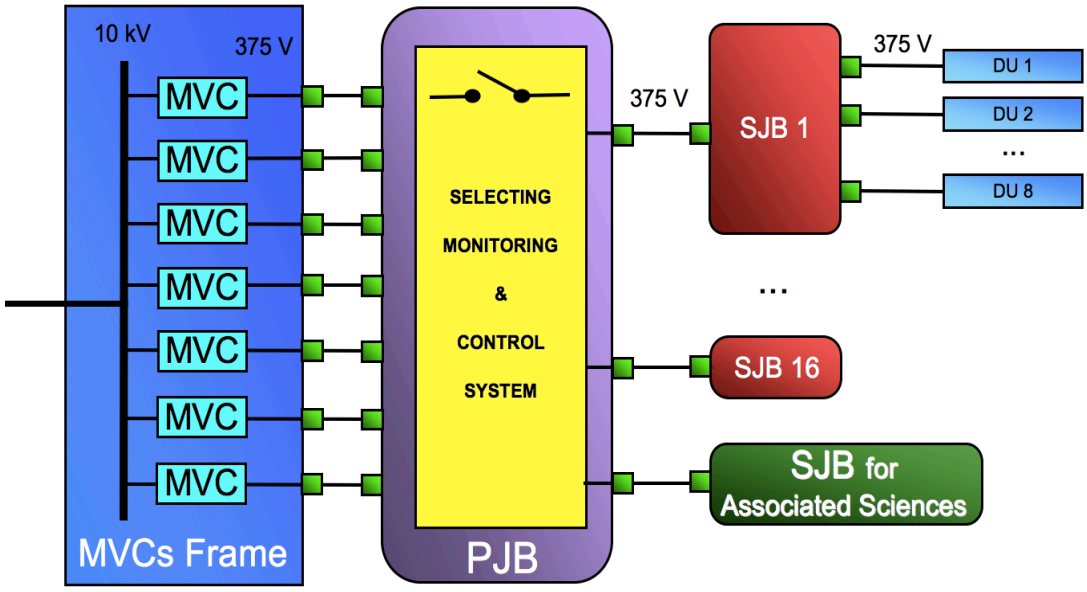

Fig. 2.34 – Block diagram of the Primary Junction Box power transmission.

The final design of the PJB is not available. Two PJBs have been developed in the framework of the projects ANTARES and NEMO. The final project will be based on the achieved experience.

The ANTARES junction box structure, illustrated in Fig. 2.35, is based on 1 m diameter titanium pressure sphere, with hemispheres separated by a central titanium cylinder ("belt") through which all power and data connections pass to the exterior.

Fig. 2.35 – The ANTARES JB on the deck of the deployment ship.

The JB internal pressure is 1 bar while the ambient external sea pressure is ~250 bar. Each hemisphere is sealed to the belt with two concentric 'O' rings. The lower hemisphere contains an oil[1]-immersed 24KVA transformer (the ANTARES power transmission is in AC) while the upper hemisphere contains the power system slow control electronics. Following component installation, the JB sphere was qualified in a 24 hour pressure test at 310 bar (20% overpressure) in the 2.5 m diameter caisson at Comex S.A., Marseille. The sphere is supported within a rectangular titanium transit cage suspended from a pivoting arm during deployment. The cage incorporated an acoustic transponder to allow triangulation of the junction box position during deployment, an electrode for the return of current to the shore, an entry guide to protect the undersea cable from scuffing during the deployment procedure, and a plugboard equipped with 16 deep sea-mateable electro-optical connectors allowing umbilical cable connections to junction box outputs using the manipulator arm of a manned or remotely operated submersible vehicle.

The NEMO Junction Box is a key element in the streamline between the shore station and the NEMO neutrino telescope. It has been built and operated, for the 4 floors NEMO-tower deployed in the NEMO test site, at 2100m depths, in front of the Catania port. It is located at the maximum depth close to the apparatus, and it is connected to one side to the MEOC originating from the coast and to the other side to the elements of the telescope. Its functions are manifold and include:

- the electrical and data transmission;
- the control of the power feedings systems connected to the JB;
- optical and electrical deep-sea mateable connectors that can be operated by Remote Operated Vehicle (ROV)

It has been designed to host and protect the opto-electronic boards, dedicated to the distribution and the control of the power supply and digitized signals, from the effects of corrosion and pressure. The JB mechanics has been produced developing an alternative design to the standard Titanium pressure vessels. The basic idea consists in decoupling the pressure and the corrosion problems. The NEMO JB is

[1] Nynas 10GBN napthalene-based transformer oil, meeting ASTM spec D3487 type 1

realized by a pressure resistant steel vessel hosted in a fibreglass container. The volume between the inner steel vessel, capable to resist to the external pressure, and the fibreglass container is filled with oil[2] in such a way that the external fibreglass container, capable to resist to long term corrosion, is in equi-pressure. This solution improves the reliability and reduces costs by avoiding the use of expensive alloys. The NEMO JB Fig. 2.36) is composed by:

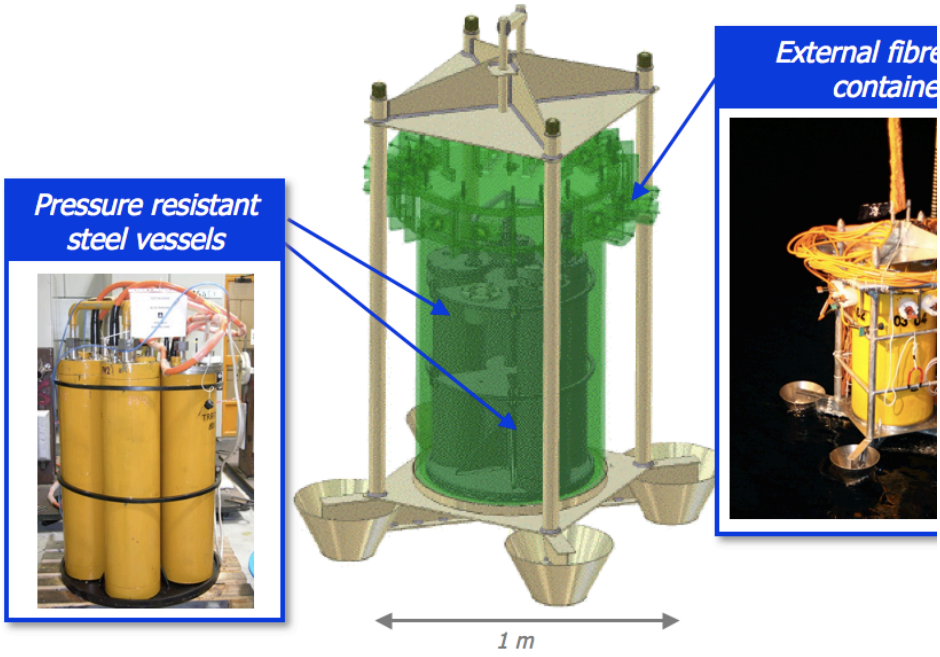

Fig. 2.36 – The NEMO Junction Box.

External components: The glass-reinforced plastic container, with an internal volume of 1.5 m^3; The external frame; One pressure compensator for the internal vessel-fibreglass oil circuit; One acoustic beacon for the positioning system;
Internal components: Four Pressure Vessels, hosting transformers and electronics boards; One Splitting Box (SB) to splice fibres and wires; The internal frame.
The aluminium external frame has been designed to guarantee feasible and reliable sea operations and deployment as well as good stability on the sea-ground; it hosts the glass-reinforced plastic container. The glass-reinforced plastic container, hosts the bulkheads of ROV operated deep-sea mateable connectors.
Several pressure vessels contain the control boards of the NEMO power supply and data transmission systems. Since the NEMO JB has been built to be operated at 2100m depths in front of the Catania port, the pressure vessels have been designed to withstand an external pressure of 350 bars. Therefore the electronics board there contained can operate when needed either in an oil bath or in air. This choice also does not lead to a significant increase of the Pressure Vessels costs and it allows an absolute flexibility in the project choices about the control electronics.

[2] DOW CORNING® 561 Silicone transformer liquid

2.1.8 Secondary Junction Box

Each SJB serves a group of no more than 8 DUs and is located close to one DU such that the distance to the other DUs is less tan 400m. Its function is to distribute the power coming from the PJB to 8 DUs. The power distribution network inside the SJB is shown in Fig. 2.37.

The SJB will host:

- a Power Feed System able to supply all the internal loads;
- a Monitoring & Control System able to switch on and off the output lines and to monitor all the lines electrical parameters;
- input and output 600 V wet mateable connector, spare included. The sum of conductors and fibres in the connector should not exceed 8 (see Fig. 2.34) to allow the use of hybrid COTS connectors.

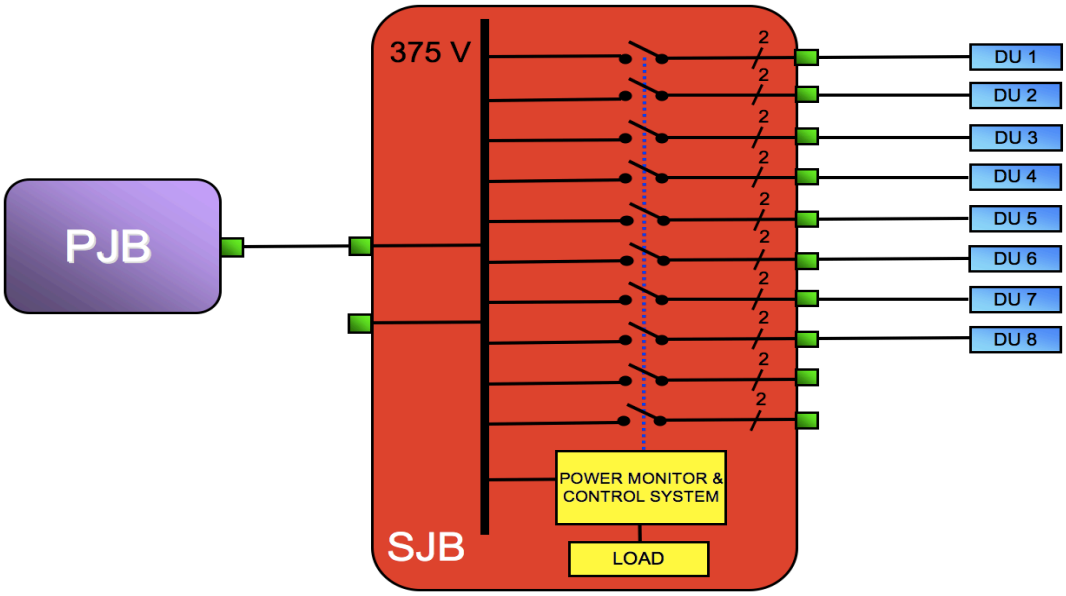

Fig. 2.37 – Block diagram of the Secondary Junction Box.

In the proposed scheme, for redundancy, each SJB is equipped with one input and two output spare connectors.

2.1.9 Power and Fiber Optical data connection with a "ring" layout

Fig. 2.38 shows, not in scale, a possible ring-configured geometry of junction boxes arranged around the circumference of the neutrino telescope. All JBs are 'primary' in the sense that they are attached to the main electro-optical cable from the shore and contain the MVC (to reduce the cable high voltage down to around 375 V DC) for supply to the detection units through radial interconnecting cables equipped with ROV wet mate-able connectors.

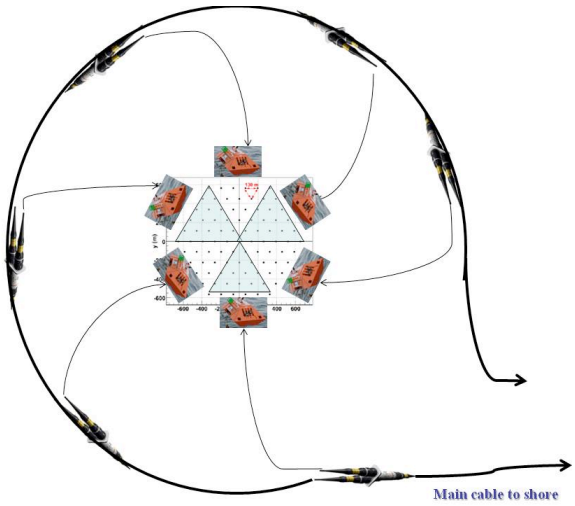

Fig. 2.38 – Possible ring geometry for sea floor infrastructure of junction boxes.

The JBs are connected to the circulating cable ring using commercially-available branching units (BUs) which allow for power to be switched individually onto each output arm. All connections of JBs and BUs in the circumferential ring use the same cable type as in the long MEOC. Furthermore, all connections are 'connector-less'; instead using 'penetrators' conforming to the Universal Joint (UJ: [REF: Universal Jointing Consortium. http://www. ujconsortium.com]) standard of industry qualified components for the termination, repair and jointing of deep sea telecommunications cables from a variety of manufacturers.

The use of UJ technology allows for the scaled deployment of the ring topology, as illustrated in Fig. 2.39-left and Fig. 2.39-right.

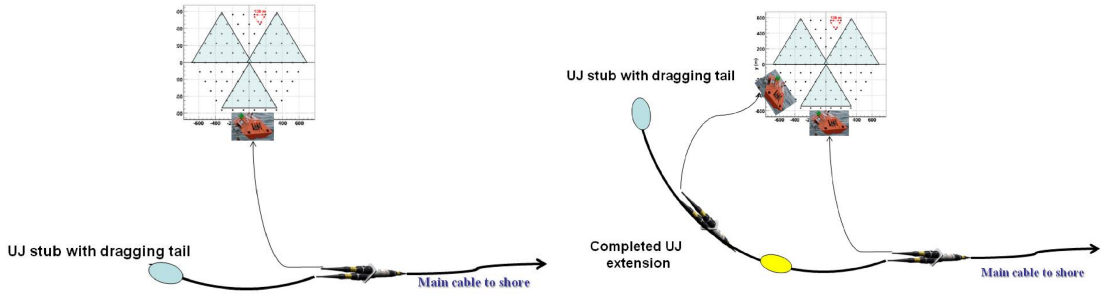

Fig. 2.39 – Illustration of the progressive deployment of a circumferential ring sea floor power and data flow topology. The drawing is not in scale.

In Fig. 2.39-left the first JB is installed together with its BU and an unconnected, recoverable cable stub terminated in a blind UJ jointing box and equipped with a 'dragging tail' allowing for later lifting with a trawled grapnel. This cable stub and its dragging tail have a length of at least twice the water depth, a factor generally considered the safe minimum for grapnel recovery by cable ship. The cable link between the BU and the JB has a similar length to allow recovery of the JB to the surface for repair without disturbance of the rest of the ring. Fig. 2.39-right illustrates the second phase of the deployment: the first formerly-blind joint box has been

replaced with a through joint to allow connection of the second BU and its dependant JB. The second cable stub will be recovered for later extension of the network as the deployment of detection units advances. It can be seen from Fig. 2.39 that the circumferential ring can connect to a second site-to-shore cable, allowing a two-fold redundancy in power path and data fibre connection to the shore. The length effects of the circumferential ring must be accommodated in the data transmission system; for example a full circumferential network deployed at 3000m depth would exceed 36 km, not including the site-to-shore cables or the BU-JB spurs.

3. Deployment and maintenance

An essential aspect of the design is the deployment concept. The detection units described below are transported and deployed into the sea as compact packages. The package is dimensioned to fit in the space of a standard transport container so as to have the possibility of final integration at distributed sites and easy transport to the sea deployment base. Each compact package is deployed in the sea, lowered to the seabed and then unfurled to deploy to the final height. It is felt that security and reliability of detector deployment must be an overriding consideration in the neutrino telescope design.

3.1 Deployment and connection

The detector deployment concept is based on the idea of deploying the DUs as compact packages to the seabed.

After the correct positioning on the seabed, the structure is connected to the sea-floor cable network. Unfurling of the DU to reach its working configuration is obtained by a actuating an acoustic release system. The DU self-unfurls under the pull provided by the buoy.

This deployment concept has several advantages:

- easy handling of the structures on-shore for loading on the surface vessel;
- reduced space occupation on the ship deck that allows to increase the number of structures to be deployed in a single operation;
- reduced time needed to lift and immerse the structure in the water, with increased safety for the operating personnel.

3.1.1 DU deployment

During the deployment the DU is a compact package with the shape of a parallelepiped and size that fits in the space of a 40’ container. This package has to be deployed and positioned at depths beyond 2500 m. The final working configuration will be reached, after deployment and connection of the structure, by remotely actuating an acoustic release system. The unfurling of the structure will be driven by the pull of the top buoy.

The operation sequence is the following:

- Lifting of the structure on the sea surface vessel deck. This operation is performed using the sea surface vessel’s deck equipment.

- Immersion of the structure in the water. This operation is performed using the sea surface vessel's deck equipment.
- Lowering of the structure close to the seabed. This operation requires a winch hosting a cable length sufficient for the site depth.
- Positioning of the structure on the seabed. The required accuracy (order of few metres) require the availability of an acoustic Long Base Line (LBL).
- Release of the structure. This operation will be performed by remotely actuating an acoustic release system placed at the end of the deployment cable.

3.1.2 Junction Boxes deployment

A design of the Junction Box has not been developed yet. For the deployment considerations we will assume that each JB is a structure with size 3 m x 3 m, a height of 2 m and a weight of approximately 3000 kg.

The deployment procedure is analogous to the one described for the tower.

3.1.3 DUs and JBs connection

After the deployment of the telescope components an ROV will be used for their connection to the seabed network for power supply and data transfer. The ROVs are described in some detail in the following paragraph "Underwater vessels".

The DUs and JBs are interconnected by a network of electro-optical cables with lengths of the order of a few hundreds metres. These cables have to be accurately laid on the seafloor along well-determined paths in order to avoid damages to this network during successive deployment of telescope components.

Interlink cables will be deployed to the seabed on dedicated drum and then laid with the ROV with a technique well tested in the installation of ANTARES.

3.2 Vessels

The surface and deep-sea vessels needed are:

- a sea surface vessel, used to transfer, deploy and install components of the deep sea neutrino telescope at the bottom of the sea, equipped with a Dynamic Positioning (DP) system;
- a deep-sea Remotely Operated Vehicle (ROV).

Other ancillary equipments are also needed to:

- precisely position the detection units on the seabed;
- deploy and lay on the seabed the cables interlinking the detection units and the junction boxes;
- operate wet mateable connectors.

3.3 Underwater vessels

Operations on the seabed will be performed by means of a Remotely Operated Vehicle (ROV) controlled from the surface.

A Remotely Operated Vehicle (ROV) is an underwater robot that allows the vehicle's operator to remain in a comfortable environment while the ROV performs the work underwater. An umbilical, or tether, carries power and command and control signals to the vehicle and the status and sensory data back to the operator topside.

A light work class ROV, like the one acquired by INFN and INGV for the PEGASO project, is adequate for the purpose. This ROV has been developed from a standard commercial vehicle by adding some dedicated equipment specifically designed for the installation of a km^3 scientific apparatus. In particular:

- the maximum operating depth has been extended down to 4000 mwd;
- the length of the tether cable between the Tether Management System (TMS) and the ROV has been increased to 250 m to allow operations inside the array;
- a system for connection/disconnection of wet-mateable connectors has been added; a connector cleaning system has been added.
- two manipulators, each with five degrees of freadom

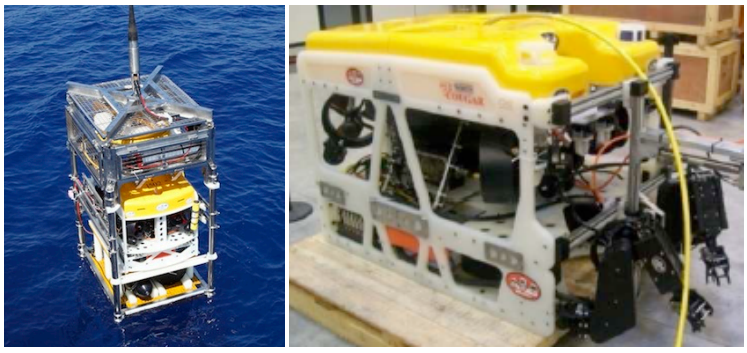

Fig. 3.1 - The light class PEGASO's ROV

Here below we list the main characteristics of the NEMO ROV.

ROV Specifications	Seaeye Cougar-XT
Depth Rating	4000 msw
Length	1515 mm
Height	790 mm
Width	1000 mm
Launch Weight	344 kg
Forward Speed	**> 3.2 knots**
Thrust Fwd	**170 kgf**
Thrust Lateral	**120 kgf**
Thrust Vertical	**110 kgf**
Payload	80 kg

Table 3-1 - The NEMO ROV characteristics

4. Common infrastructure

4.1 Electro-optical cable site-to-shore

A Main Electro-Optical Cable (MEOC) linking the Primary Junction Box to the on-shore equipment will provide the connection for power feeding and data bidirectional transmission.

4.1.1 Main electro-optical cable design

The design requirements for the KM3NeT site-to-shore cable are compatible with the standard capabilities of telecommunications cables, for which a wide range of industry-approved standard connection boxes, couplings and penetrators exist, which can be readily adapted to interface with scientific equipment. The low failure rate among the large number of such components in service suggests mean times between failures of several thousand years.

As standard, a submarine telecommunications cable has to provide a service life of at least 25 years. It must be easy to deploy and repair at sea. The longevity of the installed cable depends on minimizing the strain induced on the optical fibres.

The cable structure, which houses the optical fibres and electrical conductors, must survive both the rigors of installation (torsion, tension due to its own weight and ship movement) and the seabed conditions (high ambient pressure, abrasion risk, unsupported span, etc.).

At present all the major cable manufacturers deliver telecommunications cables with a number of fibres that does not routinely exceed 48. This is mainly due to the advent of Dense Wave-length Division Multiplexing (DWDM) technology and to the requirements of simplifying the cable mechanics. The fibre types used for submarine transmission are optimised for minimum attenuation over the full C-band (1530-1570 nm) with dispersion characteristics that depend on the application. The cable optical properties are an integral part of the optical communications system specification. The MEOC has to be equipped with standard monomode G655 fibres (MFD, LEAF or NZDSF fibres).

A monopolar system incorporates a current return via the seawater and will generally result in the smallest cable dimension and weight. Due to the extremely small resistance in the sea return this system has low power losses. Cables usable for this system are in fact the most commonly used in the telecommunications industry. To allow for the current return via the sea this system must incorporate sea electrodes both at the shore and in the deep sea. An example of such a cable is shown in Figure 4. The most significant technical problem with a DC monopolar system is the danger of corrosion of neighbouring structures and installations. Due to electrochemical reactions on the sea-return electrodes chlorine gas may be generated. Where such a system is used these issues must be addressed.

One example of such a type of electro-optical cable already deployed for deep-sea data and power transmission is the 100 km cable that will operate between the Capo Passero on-shore laboratory and the deep sea site at 3500m depths. It is a DC cable, manufactured by Alcatel-Lucent [2] and deployed in July 2007. It carries a single electrical conductor, that can be operated up to 10 kV DC allowing a power transport of more than 50 kW, and 20 single mode ITU-T G655-compatible optical fibres for data transmission. The cable total length is about 100 km.

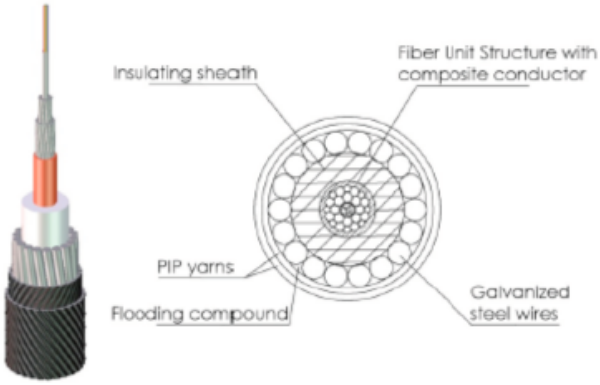

Fig. 4.1 – Internal structure of a standard monopolar submarine cable.

The KM3NeT MEOC characteristics for the data/power transmission previously described in this document are summarized in Table 4-1.

Length [km]	100
Type of power to be transmitted	DC, one polarity + sea return
Maximum Voltage [kV]	10
Maximum Current [A]	10
Power Transmission efficiency	95%
Cable resistance [Ω/km]	1
Number of fibres	48

Table 4-1 - Main Electro-Optical Cable characteristics

Submarine cable armouring is selected to be compatible with the specific route; therefore the cable mechanical characteristics are an integral component of the overall system design.
The final characteristics of the MEOC will also strongly depend on the deployment site: the cable route from the on-shore laboratory to the deep-sea site will define the length of the different MEOC parts (Double Armoured, Single Armoured, Light Weight, see Fig. 4.2) and the number of joints needed (Joint boxes DA-SA, SA-LW, DA-DA, SA-SA, LW-LW). These Joints, that are part of the long MEOC to be deployed, have to be available, and ready, during the Telescope operation, for any repair intervention will be needed.

Fig. 4.2 – Examples of different armouring on submarine cables.

4.1.2 Main electro-optical cable maintenance

The cost of a submarine cable repair at sea is substantial. However, since 1999, under the Mediterranean Cable Maintenance Agreement (MECMA) cable ships, fully equipped with Remote Operated submarine Vehicles (ROVs), are maintained on constant readiness at Catania (Italy) and La Seyne-sur-Mer (France), (Fig. 4.3). These ships provide repair services for subsea cables owned by member organisations (cable operators: around 44 as of 2009). The insurance character of this agreement offers members a repair capability for an affordable yearly contribution in proportion to the relevant cable mileage. Two of the pilot projects are members of MECMA.
The five major submarine cable manufacturing companies have formed the Universal Jointing Consortium which offers qualified and proven jointing techniques for a wide range of cable types ("Universal Joint" (UJ) and "Universal Quick Joint" (UQJ)). MECMA ships support universal jointing.
Virtually all reported submarine cable failures are due to human activity, notably fishing and anchor falls in shallow water, although natural chafing, abrasion and earthquakes in the deep ocean also occur, as shown in Fig. 4.4. To mitigate these risks, careful route planning is essential, and sea-bed burial is used where circumstances require it.

Fig. 4.3 – The MECMA consortium with the two cable-ship operatoring bases and storage depots.

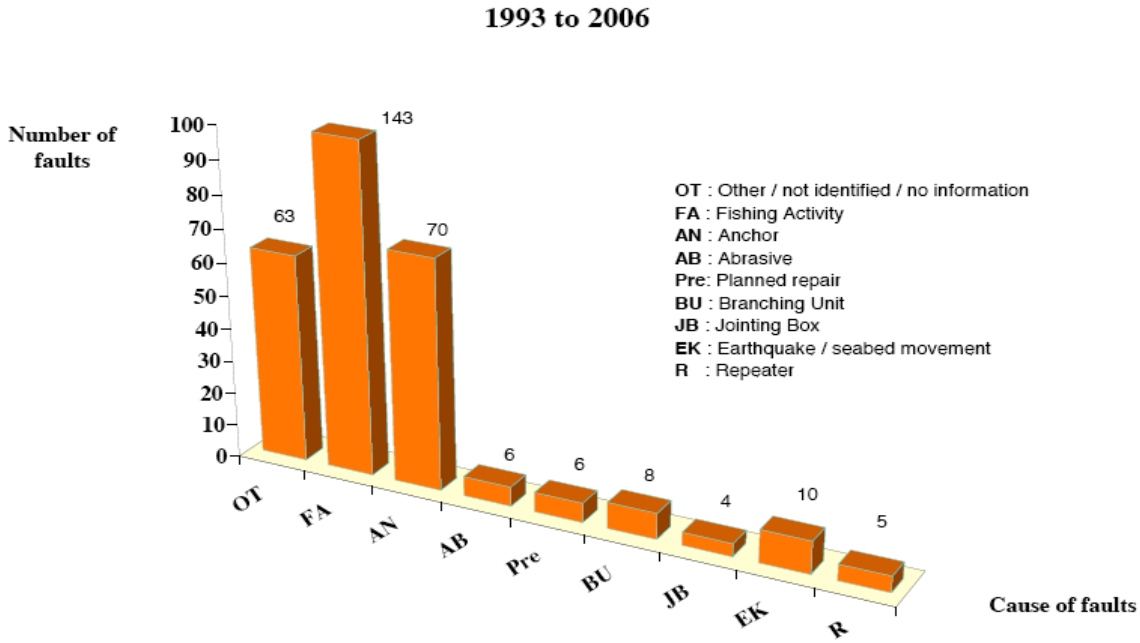

Fig. 4.4 – Submarine cables: causes of fault. (MECMA 2008.

4.2 Shore infrastructure

4.2.1 Connection to deep sea for data and power

The Shore Station Power Feeding Equipment (PFE) will provide the connection to the local utility power of both the of the off-shore and on-shore components of the Telescope. The PFE will also act as emergency back-up power storage, the AC and DC monitoring and control, a protection against lightning, surge and spike. The PFE will provide the connection to the current return electrode and the connection to the KM3NeT backbone cable. The PFE will utilize the local public utility 400 VAC, convert it to 240VAC for the low voltage equipment and to medium voltage DC for distribution to the seafloor equipment. In order to maintain the availability of the KM3NeT network during occasional power interruptions, a backup power system will be required to provide power during these interruptions. An UPS would be provided for sufficient time to reliably start a motor generator and then the generator would provide power until the utility power was restored.

The primary function of the PFE is to generate the nominal -10kVDC for transmission to the seafloor cable network. This will require a 400VAC/10kVDC power supply unit (PSU).

The PSU will have 2 output connections: the single conductor backbone cable and the current return electrode.The backbone cable conductor will be connected to the negative terminal of the PSU and the electrode will be connected to the positive terminal of the PSU. This polarity is used to minimize consumption of the remote seafloor electrodes (cathodes) that are difficult to maintain.

The shore electrode (anode) will be consumed but this can be made arbitrarily large and can be maintained/replaced, if necessary.